iScience

CellPress
OPEN ACCESS

Article

Lipopolysaccharide increases bitter taste sensitivity via epigenetic changes in *Tas2r* gene clusters

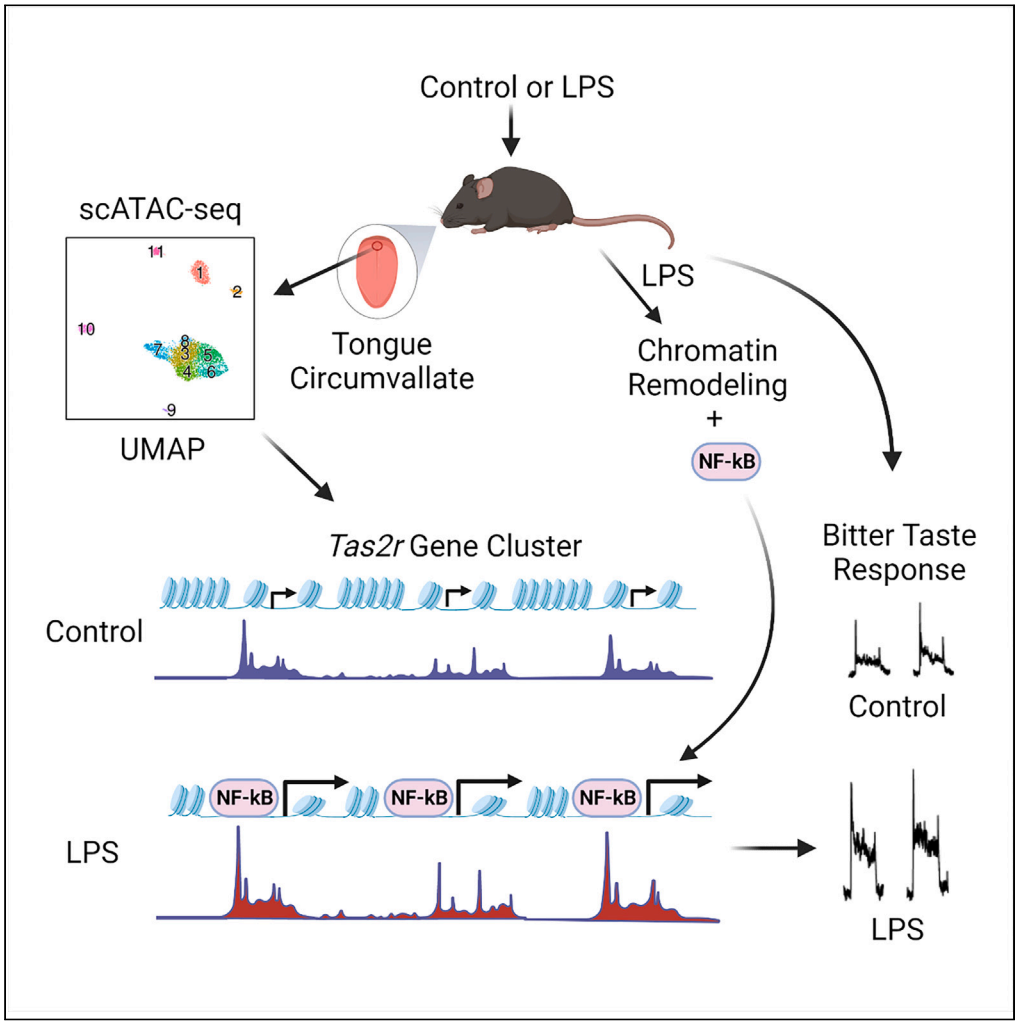

Cailu Lin, Masafumi Jyotaki, John Quinlan, ..., Robert F. Margolskee, Danielle R. Reed, Hong Wang

hwang@monell.org

Highlights

Lipopolysaccharide (LPS) selectively augments bitter taste response in mice

Expression of the majority of *Tas2r* genes is stimulated by LPS in taste tissues

scATAC-seq revealed that LPS increases chromatin accessibility to *Tas2r* genes

We identify a mechanism connecting *Tas2r* gene regulation to altered bitter taste

Lin et al., iScience *26*, 106920
June 16, 2023
https://doi.org/10.1016/j.isci.2023.106920

iScience

CellPress
OPEN ACCESS

Article

Lipopolysaccharide increases bitter taste sensitivity via epigenetic changes in *Tas2r* gene clusters

Cailu Lin,[1,6] Masafumi Jyotaki,[1,6,7] John Quinlan,[1,8] Shan Feng,[1,9] Minliang Zhou,[1] Peihua Jiang,[1] Ichiro Matsumoto,[1] Liquan Huang,[1,2] Yuzo Ninomiya,[1,3,4,5] Robert F. Margolskee,[1] Danielle R. Reed,[1] and Hong Wang[1,10,*]

SUMMARY

T2R bitter receptors, encoded by *Tas2r* genes, are not only critical for bitter taste signal transduction but also important for defense against bacteria and parasites. However, little is known about whether and how *Tas2r* gene expression are regulated. Here, we show that in an inflammation model mimicking bacterial infection using lipopolysaccharide, the expression of many *Tas2rs* was significantly upregulated and mice displayed markedly increased neural and behavioral responses to bitter compounds. Using single-cell assays for transposase-accessible chromatin with sequencing (scATAC-seq), we found that the chromatin accessibility of *Tas2rs* was highly celltype specific and lipopolysaccharide increased the accessibility of many *Tas2rs*. scATAC-seq also revealed substantial chromatin remodeling in immune response genes in taste tissue stem cells, suggesting potential long-lasting effects. Together, our results suggest an epigenetic mechanism connecting inflammation, *Tas2r* gene regulation, and altered bitter taste, which may explain heightened bitter taste that can occur with infections and cancer treatments.

INTRODUCTION

T2Rs (encoded by *Tas2rs* in mice or *TAS2Rs* in humans) were identified more than twenty years ago as bitter taste receptors.[1] However, their functions extend far beyond taste signal transduction. T2Rs expressed in solitary chemosensory cells have been shown to play important roles in recognizing bacterial quorum-sensing molecules and are involved in bacterial defense in the upper airway.[2–4] T2Rs in gut tuft cells are involved in defense against parasites.[5] Of interest, thymic tuft cells also express an array of *Tas2r* genes and may be involved in T cell development.[6] T2Rs have also been implicated in allergies.[7] These studies suggest that T2Rs are an integral part of immune responses. Although it is well known that genes involved in immunity are often regulated by inflammatory stimuli, whether and how the expression of *Tas2rs* are regulated by inflammation remain to be determined.

Bitter taste is a basic taste quality and believed to serve as a warning signal for potentially harmful compounds in food. To humans and many animal species, bitter taste is innately aversive,[8] even though humans can learn to accept some bitterness for pharmaceutical or nutritional reasons. Bitter taste sensitivity is linked to food preference and intake and influences the consumption of vegetables and alcohol.[9–11] Genetic polymorphisms in *TAS2R* genes contribute to variations in bitter taste sensitivity.[12] Some diseases also appear to affect bitter taste. Heightened or persistent bitter or metallic taste, a type of taste distortions, can occur in patients with infections or undergoing cancer treatments and contributes to food aversion and low quality of life.[13,14] In traditional Chinese medicine, oral bitterness is an indication used for disease diagnosis. However, the underlying cause for the increased bitter taste sensitivity is unknown.

Embedded in the oral epithelium and exposed to the oral cavity, taste buds are vulnerable to infections.[15] Our previous studies showed that taste cells are equipped with proteins in innate immune pathways, including multiple Toll-like receptors (TLRs) for detecting pathogen-derived molecules.[16,17] Type II taste bud cells were shown to play immune surveillance roles in the oral mucosa.[18] Activation of innate immune

[1]Monell Chemical Senses Center, 3500 Market St., Philadelphia, PA 19104, USA

[2]Institute of Cellular and Developmental Biology, College of Life Sciences, Zhejiang University, Hangzhou, Zhejiang 310058, China

[3]Division of Sensory Physiology, Research and Development Center for Five-Sense Device, Kyushu University, Fukuoka, Japan

[4]Okayama University, Okayama, Japan

[5]Oral Science Research Center, Tokyo Dental College, Tokyo, Japan

[6]These authors contributed equally

[7]Present address: Japan Tobacco Inc., Tobacco Science Research Center, 6-2 Umegaoka, Aoba-ku, Yokohama, Kanagawa 227-8512, Japan

[8]Present address: University of Maryland School of Medicine and Fischell Department of Bioengineering, University of Maryland, College Park, MD, USA

[9]Present address: College of Pharmaceutical Sciences and Chinese Medicine, Southwest University, Chongqing, China

[10]Lead contact

*Correspondence: hwang@monell.org

https://doi.org/10.1016/j.isci.2023.106920

pathways changes the expression of numerous genes,[19] which is protective against infections but can also lead to pathology. Whether innate immune responses directly regulate *Tas2r* gene expression and bitter taste is unclear.

In this study, we show that lipopolysaccharide (LPS), a pathogen-associated molecular pattern (PAMP) in bacteria and a ligand for TLR4, induced the expression of the majority of *Tas2rs* and markedly increased neural and behavioral responses to bitter compounds. Using the single-cell assay for transposase-accessible chromatin with sequencing (scATAC-seq) approach, we showed that the accessibility of *Tas2r* genomic regions was tightly controlled and mostly limited to type II taste cells. However, LPS treatment significantly increased chromatin accessibility of many *Tas2rs*, indicating an epigenetic mechanism for heightened bitter taste under disease conditions. We also found that the promotor regions of some *Tas2rs* contained potential binding sites for NF-κB, a transcription factor that upregulates transcription of many inflammation-related genes. In addition, systemic LPS administration resulted in broad changes in the chromatin accessibility landscape in taste tissue stem cells, suggesting potentially long-lasting effects.

RESULTS

Bitter taste responses were markedly elevated in LPS-induced inflammation

To investigate whether *Tas2r* gene expression and bitter taste are regulated by innate immune responses, we used the well-established systemic inflammation model induced by LPS. Bacterial LPS activates TLR4-mediated signaling pathway and stimulates the production and secretion of an array of inflammatory cytokines.[20] This inflammatory cascade also occurs in taste tissues.[17,21] Here, we carried out experiments to measure behavioral and neural responses to taste compounds in this inflammation model (Figure 1A). As shown in Figure 1B, we found that LPS-treated mice displayed strong avoidance behavior to the bitter compound quinine compared to mice that received phosphate-buffered saline (PBS; a vehicle control). To confirm that the hyper-avoidance behavior to quinine was because of increased peripheral bitter taste responses, we conducted gustatory nerve recording experiments from both chorda tympani and glossopharyngeal nerves that innervate taste buds in the anterior and posterior parts of the tongue, respectively. Results from these experiments demonstrated that, indeed, LPS treatment induced significantly stronger gustatory nerve responses to bitter compounds (Figures 1C and S1B). Surprisingly, even though we detected dampened behavioral responses to sucrose in LPS-treated mice in brief-access tests (Figure S1A), the chorda tympani and glossopharyngeal nerve responses to sucrose, as well as to several other sweet compounds, did not show detectable differences in LPS-treated mice compared to control mice (Figures 1D and S1B). This result suggests that the reduced behavioral responses to sweet compounds were likely because of brain-mediated mechanisms, consistent with previous reports.[22] We also did not observe significant differences in taste nerve responses to umami or salt compounds (Figures 1E, 1F, and S1B). LPS-treated mice showed reduced responses to sour compounds only at high concentrations of HCl and citric acid in chorda tympani recordings (Figure 1F). Together, our results show that LPS-induced inflammation selectively alters bitter taste responses through peripheral mechanisms.

LPS stimulated the expression of the majority of *Tas2rs* in the taste epithelium

To investigate the underlying mechanism for the LPS-induced hyper-responsiveness to bitter compounds, we analyzed *Tas2r* gene expression in the taste epithelium from circumvallate and foliate taste papillae by real-time quantitative reverse-transcription polymerase chain reaction (qRT-PCR). As shown in Figure 2A, LPS treatment stimulated expression of the majority of *Tas2rs*. On day 3 after LPS injection, expression of more than 20 mouse *Tas2rs* was significantly up-regulated by at least 2-fold. We selected several *Tas2rs*, including *Tas2r102*, *108*, *110*, *116*, *124*, and *137*, and analyzed their expression across several time points after LPS injection. Elevated expression of *Tas2r102*, *110*, *116*, and *137* peaked on day 3 after LPS injection (Figure 2B), whereas expression of *Tas2r108* and *124*, as well as *Trpm5*, peaked on day 5 (Figure 2C). Expression of *Nfkb1*, a transcription factor involved in inflammatory responses, was also mildly elevated on days 1–5 and returned to control level on day 10 (Figure 2C). Of note, 8 of the 10 highly induced *Tas2rs* (>3-fold induction) are located in a closely linked region on mouse chromosome 6 (Figure 2D).

scATAC-seq identified taste and nontaste cell clusters

scATAC-seq can reveal gene regulatory mechanisms, but its use for studying taste receptor gene expression has not been reported. To better understand *Tas2r* gene regulation, we performed scATAC-seq experiments. We isolated single-cell nuclei from the circumvallate epithelium of PBS- (vehicle control) and

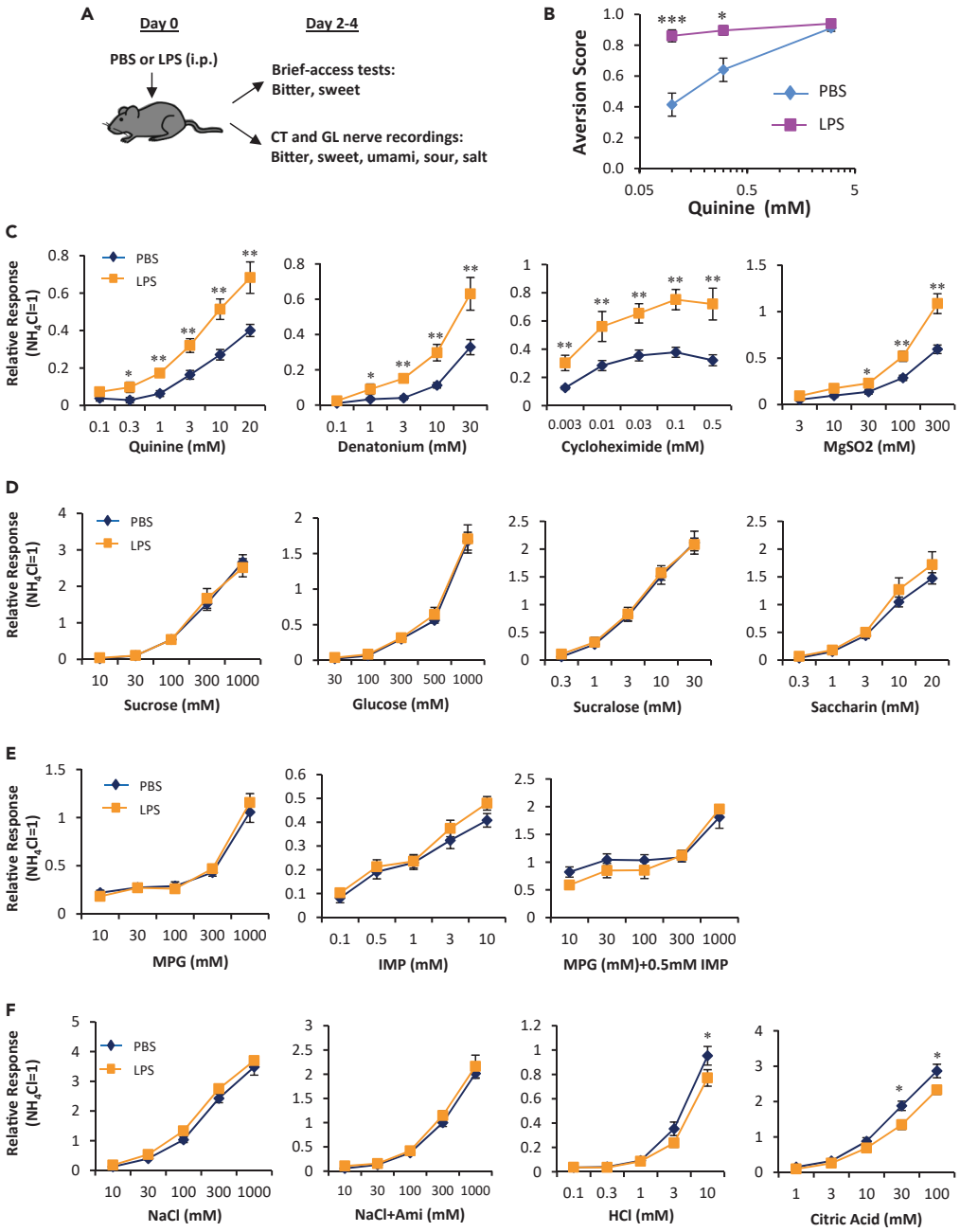

Figure 1. LPS induced neural and behavioral responses to bitter compounds

(A) Timeline of experiments. CT, chorda tympani nerve; GL, glossopharyngeal nerve.

(B) LPS increased behavioral responses to quinine in brief-access tests. The taste behavioral tests were performed on day 3 after LPS or PBS (control) injection. Aversion scores were calculated as 1 – the lick ratio (tastant licks/water licks). Data are means ± SEM. *p<0.05; ***p<0.005 (ANOVA with post hoc t tests). N = 8–10 mice per group.

(C–F) LPS selectively increased chorda tympani nerve responses to bitter compounds (C) but not to sweet (D), umami (E), salty or sour compounds (F). MPG, monopotassium glutamate; IMP, inosine-5′-monophosphate; Ami, amiloride. Gustatory nerve recordings were conducted on day 3 after PBS or LPS injection. Data are means ± SEM. *p<0.05; **p<0.01 (ANOVA with post hoc *t* tests). N = 6–12 mice per group.

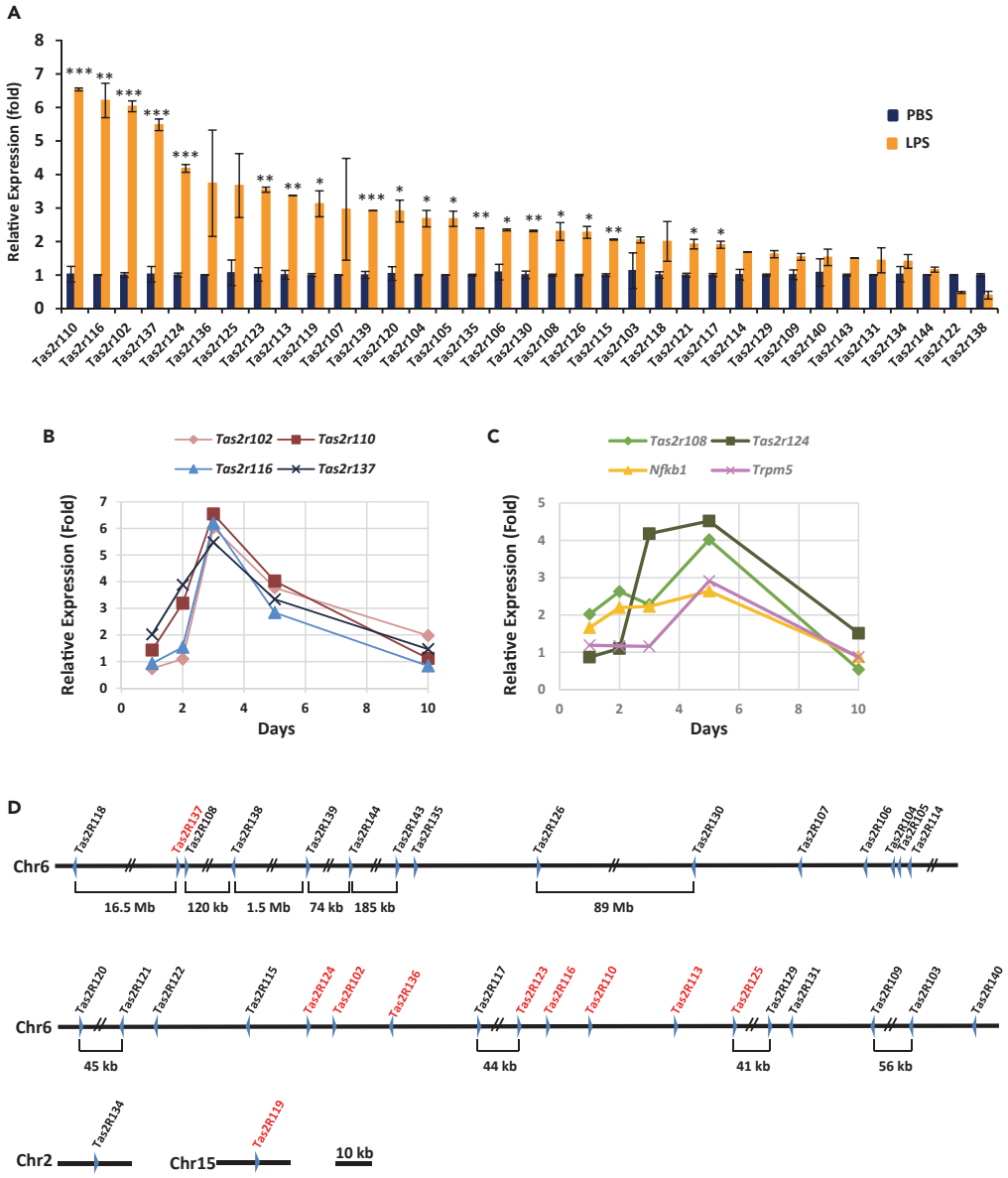

Figure 2. LPS stimulated expression of the majority of *Tas2rs*

(A) qRT-PCR analysis of mRNA levels of 35 mouse *Tas2rs* in the circumvallate and foliate epithelium 3 days after LPS or PBS injection. Gene expression in PBS samples was set to 1. β-Actin was used as the endogenous control. Data are means ± SEM. *p<0.05; **p<0.01; ***p<0.005 (t tests). Six mice per group were used.

(B and C) Time course of LPS-induced expression of six *Tas2rs*, *Nfkb1*, and *Trpm5*. qRT-PCR experiments were performed as described in A. Six mice per group per time point were used.

(D) Schematic illustration of *Tas2r* distribution on mouse chromosomes. Red indicates that the gene was induced >3-fold by LPS. Blue arrowheads indicate direction of *Tas2r* gene transcription.

LPS-treated mice. The scATAC-seq datasets were processed using the ArchR package, which provided comprehensive features for analyzing scATAC-seq data.[23] Quality checks of the data are shown in Figure S2. The overall quality and the Simpson diversity index of the datasets from the control (PBS) and LPS-treated mice were comparable. In total, 3424 and 4032 nuclei from PBS- and LPS-treated mice, respectively, were included in downstream analyses (Figure S2E). With the combined dataset, we performed uniform manifold approximation and projection (UMAP) dimension reduction and clustering and identified 11 cell clusters (Figure 3A). The number and percentage of cells in each cell cluster are listed in Table S1.

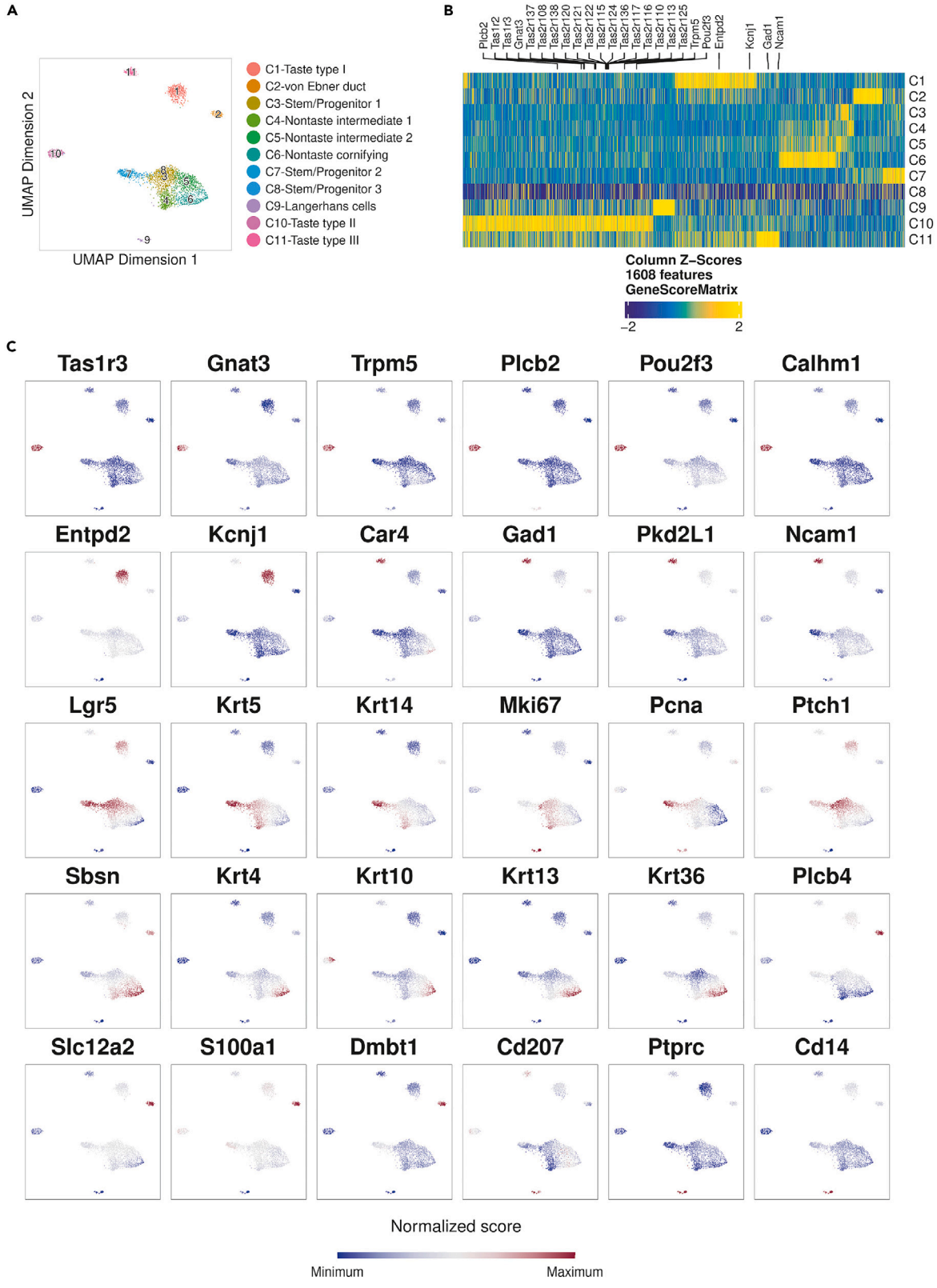
A
UMAP Dimension 2
UMAP Dimension 1
C1-Taste type I
C2-von Ebner duct
C3-Stem/Progenitor 1
C4-Nontaste intermediate 1
C5-Nontaste intermediate 2
C6-Nontaste cornifying
C7-Stem/Progenitor 2
C8-Stem/Progenitor 3
C9-Langerhans cells
C10-Taste type II
C11-Taste type III
B
Plcb2
Tas1r2
Tas1r3
Gnat3
Tas2r137
Tas2r108
Tas2r138
Tas2r120
Tas2r121
Tas2r122
Tas2r115
Tas2r124
Tas2r136
Tas2r117
Tas2r116
Tas2r110
Tas2r113
Tas2r125
Trpm5
Pou2f3
Entpd2
Kcnj1
Gad1
Ncam1
C1
C2
C3
C4
C5
C6
C7
C8
C9
C10
C11
Column Z-Scores
1608 features
GeneScoreMatrix
−2
2
C
Tas1r3
Gnat3
Trpm5
Plcb2
Pou2f3
Calhm1
Entpd2
Kcnj1
Car4
Gad1
Pkd2L1
Ncam1
Lgr5
Krt5
Krt14
Mki67
Pcna
Ptch1
Sbsn
Krt4
Krt10
Krt13
Krt36
Plcb4
Slc12a2
S100a1
Dmbt1
Cd207
Ptprc
Cd14
Normalized score
Minimum
Maximum

Figure 3. scATAC-seq identified taste and nontaste cell clusters

(A) UMAP plot of cell clusters of circumvallate epithelia from control mice. The inferred identities of the cell clusters are shown on the right.

(B) A heatmap of gene scores of identified significant marker genes across cell clusters. Some well-characterized marker genes for type I, II, and III taste bud cells are shown on top.

(C) Feature plots of cell-type marker genes that show gene scores in cell clusters. Gene names are shown on the top of each plot.

Next, we performed in-depth analysis of the dataset from control mice. We calculated gene scores (or gene activity scores) based on chromatin accessibility using algorithms in ArchR.[23] Chromatin accessibility of individual genes strongly correlates with, and thus can be used as a proxy for, gene expression.[23,24] To infer the identities of the cell clusters, we generated a gene score heatmap (Figure 3B) and identified marker genes for each cell cluster. The UMAP plots for well-characterized cell-type markers are shown in Figure 3C.

Three well-separated cell clusters on the UMAP (Figure 3A), C1, C10, and C11, showed high gene scores for many taste bud cell markers corresponding to taste cell types I, II, and III, respectively.[25,26] *Entpd2* and *Kcnj1* encode type I taste cell markers[27,28] and showed the highest gene scores in the C1 cluster (Figures 3B and 3C and Table S3), indicating this cell cluster represents type I taste cells. *GAD2* is also enriched in the C1 cluster (Table S3), consistent with a recent report showing selective expression of this gene in type I taste cells.[29] Similarly, many type II taste cell marker genes, such as *Tas1rs*, *Tas2rs*, *Gnat3*, *Trpm5*, *Plcb2*, *Pou2f3*, and *Calhm1*,[26] had the highest gene scores in the C10 cluster (Figures 3B and 3C), indicating the C10 cluster denotes type II taste receptor cells. *Car4*, *Pkd2l1*, *GAD1*, and *Ncam1* encode well-established type III taste bud cell markers,[25,30] and all showed highest gene scores in the C11 cluster (Figures 3B and 3C). Among the three clusters, the percentages of cells in C1 (type I), C10 (type II), and C11 (type III) were 61.6%, 23%, and 15.4%, respectively. This relative abundance of cells was similar to previously reported proportions of type I, II, and III cells in taste buds,[31,32] further supporting our annotations of these clusters. Moreover, this analysis identified many candidate genes that showed selective gene scores in the three types of taste bud cells (Table S3).

The C2 cluster is also a well-separated cell cluster on UMAP and shows high gene scores for marker genes of salivary glands. The von Ebner gland, a minor salivary gland, secretes saliva that drains into the circumvallate trenches through gland ducts. In preparing circumvallate epithelium for scATAC-seq, the top portions of the von Ebner gland ducts were also included. Our analysis showed that the C2 cluster was enriched with *Slc12a2*, *S100a1*, *Plcb4*, and *Dmbt1* (i.e., Ebnerin) (Figure 3C); all have been shown to be selectively expressed in salivary glands.[33,34] *Dmbt1* was shown to be abundantly expressed in von Ebner gland duct cells,[34,35] indicating the C2 cluster represents von Ebner gland duct cells.

The small C9 cell cluster showed high gene scores for CD207 (i.e., Langerin), a well-established marker for Langerhans cells (i.e., epidermis-resident macrophages).[36] *Ptprc* (encodes CD45) and *Cd14* are marker genes for hematopoietic-derived cells and macrophages, respectively, and both showed high gene scores in C9, consistent with the identity of Langerhans cells (Figure 3C).

Collectively, *Lgr5*, *Krt5*, *Krt14*, and *Ptch1*, genes that encode markers for taste stem/progenitor cells, showed high gene scores in C3, C7, and C8 clusters (Figure 3C), indicating these clusters represent stem/progenitor cells in the taste tissue. Both *Mki67* and *Pcna* are cell proliferation marker genes, but *Mki67* is more specific for actively proliferating cells.[37,38] Considering the relative gene scores of the above markers, C7 most likely represents a stem cell cluster because of its high gene score for *Lgr5* but medium score for *Mki67*. C3 and C8 most likely represent transient amplifying cell clusters with high gene scores for *Mki67* and *Ptch1* but medium scores for *Lgr5* (Figure 3C). Only a small number of cells in control mice were assigned to the C8 cluster, but LPS treatment dramatically increased the number of cells in this cluster (Table S1). These data suggest that the C8 cluster could represent a transient cell state between taste progenitor cells and postmitotic taste precursor cells. During normal taste bud turnover, the transition between the cell states proceeds swiftly. However, this transition may be suppressed by LPS-induced inflammation, consistent with our previous reports that showed LPS treatment inhibited taste bud cell renewal.[21] Furthermore, we found that *Ugt2a1*, a candidate gene related to COVID-19-induced taste and smell loss,[39] is enriched in the C3 cluster of stem/progenitor cells (Table S3), suggesting a possible role of *Ugt2a1* in taste cell turnover and renewal.

Clusters C4, C5, and C6 showed increasing enrichment for markers of cornifying, terminally differentiating keratinocytes (Table S3). The UMAP plots for some of the marker genes, including *Sbsn*, *Krt4*, *Krt10*, *Krt13*,

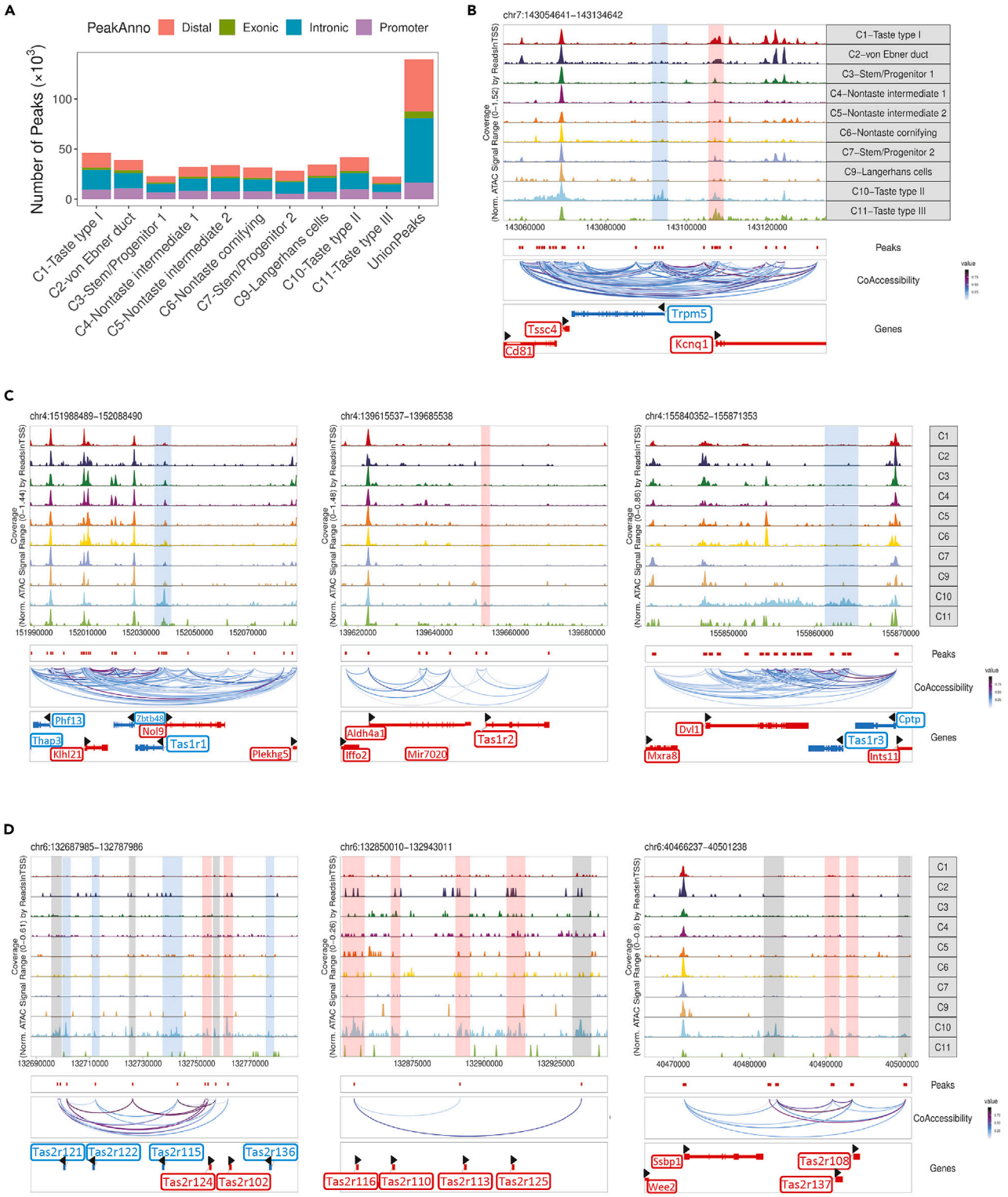

Figure 4. scATAC-seq identified putative regulatory regions in taste receptor and signaling genes

Analysis of chromatin-accessible peaks from control mice.

(A) Distribution of accessible peaks in distal, exonic, intronic, and promoter regions. PeakAnno, peak annotation.

Figure 4. *Continued*

(B–D) Chromatin-accessible peaks in the genomic regions of *Trpm5* and *Kcnq1* (B), *Tas1rs* (C), and some *Tas2rs* (D). Gene symbols in red indicate genes transcribed in the forward direction, and their cluster-selective accessible peaks are highlighted in pink. Gene symbols in blue indicate genes transcribed in the reverse direction, and their cluster-selective accessible peaks are highlighted in blue. Gray bars in D highlight type II cell-selective peaks in intergenic regions. Black arrowheads also indicate the direction of gene transcription. TSS, transcription start site.

and *Krt36*,[40–42] are shown in Figure 3C. Cells in the C4 cluster also exhibited relatively high gene scores for *Krt5*, *Krt14*, and *Mki67*, indicating these cells may still have proliferating capacity. Conversely, the C6 cluster displayed high gene scores for the above-mentioned terminal differentiation markers of keratinocytes and most likely represents cornifying nontaste epithelial cells, whereas the C5 cluster showed an intermediate phenotype (Figure 3C).

With the identified significant marker genes for each cell cluster, we performed pathway enrichment analyses using g:Profiler[43,44] and Cytoscape[45]/EnrichmentMap[46] software. As expected, type II taste cells showed strong pathway enrichment for GPCR-mediated taste perception, whereas type III cells were enriched with synaptic activities (Figures S3B and S3C), consistent with the functions of these taste cells. Of interest, type I taste cells displayed enrichment for protein secretion, hormone secretion, and hormone transport (Figure S3A), suggesting these cells may play important physiological roles in taste buds, such as connecting hormonal responses to taste sensation.

scATAC-seq revealed cell-type-specific chromatin accessibility of *Tas2r* genes

Chromatin accessibility represents a fundamental feature of cell identity. To date, the chromatin accessibility landscape of taste bud cells has not been reported. To gain insights into cell-type-specific gene expression regulation, we performed chromatin-accessible peak calling using ArchR. Figure 4A shows peak distribution in different genomic regions. Most peaks are located in the intronic and distal regions, followed by the promoter regions, whereas the exonic regions have the least number of peaks. This pattern of peak distribution is very similar to that observed in other types of tissues, such as retina and brain.[24,47]

The *Tas2r* bitter receptor genes form several gene clusters in the genome (Figure 2D). The chromatin accessibility landscapes of some *Tas2rs* are shown in Figures 4D and S4A. *Tas2rs* showed highly selective accessibility in type II taste cells. Moreover, we identified several intergenic peaks in the *Tas2r* genomic regions that showed selective accessibility in type II cells (gray bars, Figures 4D and S4A). These peaks and the neighboring *Tas2rs* peaks share strong co-accessibility, suggesting these intergenic peaks could contain putative *cis*-regulatory elements, such as enhancers for *Tas2rs*.

We also analyzed chromatin accessibility of other well-known genes involved in taste reception and signaling. Figure 4B shows chromatin-accessible peaks for *Trpm5*, a gene encoding an ion channel required for sweet, umami, and bitter taste signaling.[48] Chromatin-accessible peaks were enriched in the promoter region and the transcription start site (TSS) only in type II taste cells. In contrast, the adjacent gene *Kcnq1* (Figure 4B) showed high chromatin accessibility in its promoter and TSS regions in all three taste cell clusters (C1, C10, and C11 clusters), consistent with the expression of *Kcnq1* (encodes a pan-taste-cell marker).[49,50] In addition, co-accessibility analysis showed that many peaks in the surrounding regions of *Trpm5* were strongly co-accessible with the *Trpm5* peaks, suggesting these genomic regions may contain putative regulatory elements for *Trpm5* gene expression.

Similarly, the three *Tas1rs* that encode umami and sweet taste receptors showed accessible peaks selectively in type II taste cells (Figure 4C). Furthermore, many other type II taste cell marker genes, such as *Gnat3*, *Plcb2*, *Pou2f3*, and *Calhm1*, also exhibited selective chromatin-accessible peaks in type II taste cells (Figure S4B).

Genes encoding markers for type I and III taste cells, such as *Entpd2*, *Kcnj1*, *Car4*, *GAD1*, and *Pkd2l1*, showed peaks selectively either in type I or type III taste cells (Figure S5). Of interest, *Otop1*, which encodes a recently identified sour taste receptor,[51] showed enriched accessibility in both type I and type III cell clusters (Figure S5B). However, at least one peak within an intronic region of *Otop1* showed specific accessibility in type III cells. Again, such peaks could contain *cis*-regulatory elements for *Otop1* gene expression in type III taste cells.

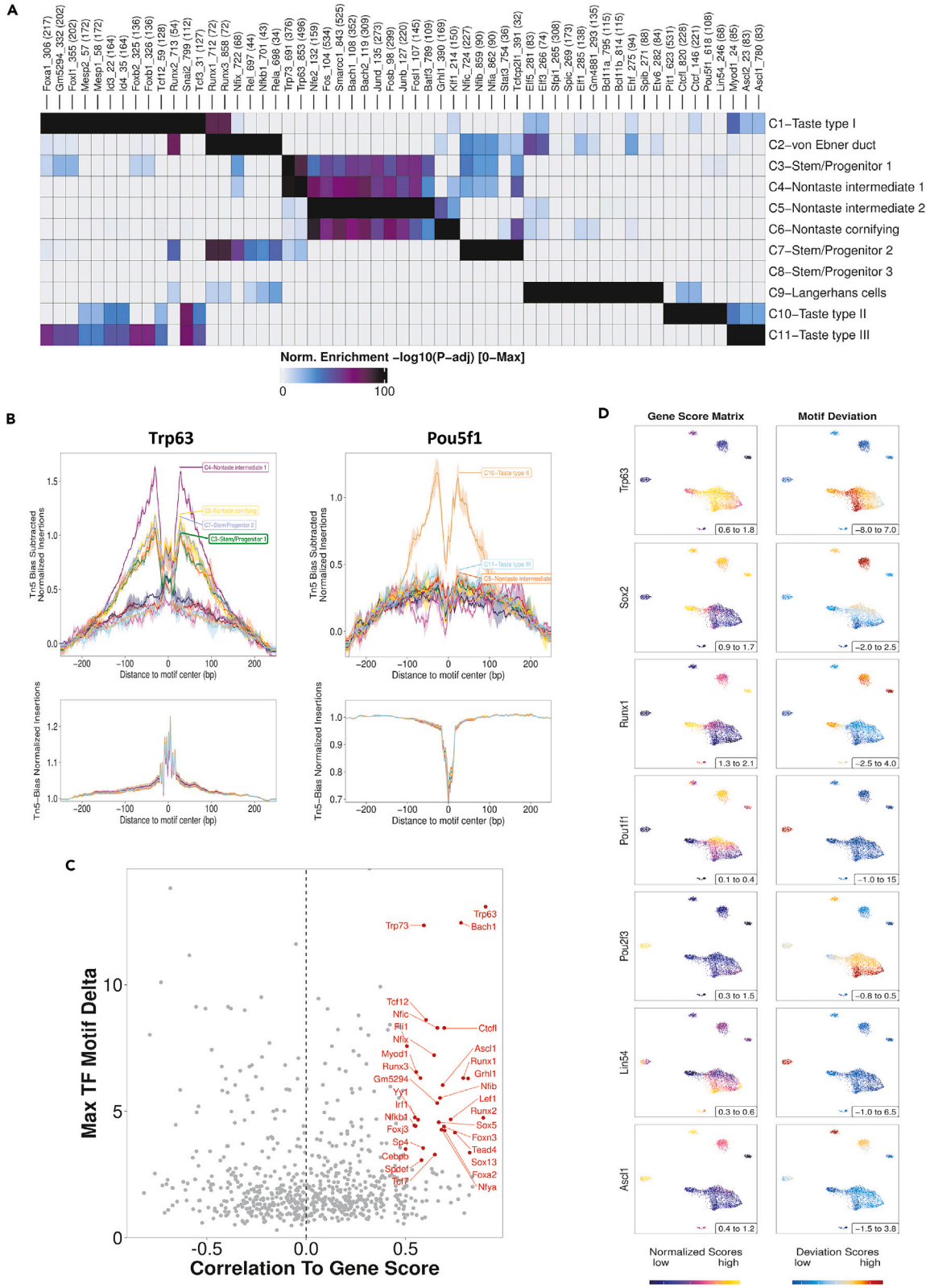
A
Foxa1_306 (217)
Gm5294_332 (202)
Foxl1_355 (202)
Mesp2_57 (172)
Mesp1_58 (172)
Id3_22 (164)
Id4_35 (164)
Foxb2_325 (136)
Foxb1_326 (136)
Tcf12_59 (128)
Runx2_713 (54)
Snai2_799 (112)
Tcf3_31 (127)
Runx1_712 (72)
Runx3_858 (72)
Nfix_722 (68)
Rel_697 (44)
Nfkb1_701 (43)
Rela_698 (34)
Trp73_691 (376)
Trp63_853 (496)
Nfe2_132 (159)
Fos_104 (534)
Smarcc1_843 (525)
Bach1_108 (352)
Bach2_119 (309)
Jund_135 (273)
Fosb_98 (299)
Junb_127 (220)
Fosl1_107 (145)
Batf3_789 (109)
Grhl1_390 (169)
Klf1_214 (150)
Nfic_724 (227)
Nfib_859 (90)
Nfia_862 (90)
Stat3_754 (36)
Tcfcp2l1_391 (32)
Elf5_281 (83)
Elf3_266 (74)
Slpi1_265 (308)
Spic_269 (173)
Elf1_285 (138)
Gm4881_293 (135)
Bcl11a_795 (115)
Bcl11b_814 (115)
Ehf_275 (94)
Spib_271 (88)
Etv6_282 (84)
Pit1_623 (531)
Ctcfl_820 (228)
Ctcf_146 (221)
Pou5f1_618 (108)
Lin54_246 (68)
Myod1_24 (85)
Ascl2_23 (83)
Ascl1_780 (83)
C1–Taste type I
C2–von Ebner duct
C3–Stem/Progenitor 1
C4–Nontaste intermediate 1
C5–Nontaste intermediate 2
C6–Nontaste cornifying
C7–Stem/Progenitor 2
C8–Stem/Progenitor 3
C9–Langerhans cells
C10–Taste type II
C11–Taste type III
Norm. Enrichment –log10(P–adj) [0–Max]
0
100
B
Trp63
Pou5f1
C4–Nontaste intermediate 1
C6–Nontaste cornifying
C7–Stem/Progenitor 2
C3–Stem/Progenitor 1
C10–Taste type II
C11–Taste type III
C5–Nontaste intermediate 2
Tn5 Bias Subtracted Normalized Insertions
Tn5–Bias Normalized Insertions
Distance to motif center (bp)
C
Max TF Motif Delta
Correlation To Gene Score
Trp63
Trp73
Bach1
Tcf12
Nfic
Fli1
Ctcfl
Nfix
Ascl1
Myod1
Runx1
Runx3
Grhl1
Gm5294
Nfib
Yy1
Lef1
Irf1
Runx2
Nfkb1
Sox5
Foxj3
Foxn3
Sp4
Tead4
Cebpb
Sox13
Spdef
Foxa2
Tcf7
Nfya
D
Gene Score Matrix
Motif Deviation
Trp63
Sox2
Runx1
Pou1f1
Pou2f3
Lin54
Ascl1
0.6 to 1.8
–8.0 to 7.0
0.9 to 1.7
–2.0 to 2.5
1.3 to 2.1
–2.5 to 4.0
0.1 to 0.4
–1.0 to 15
0.3 to 1.5
–0.8 to 0.5
0.3 to 0.6
–1.0 to 6.5
0.4 to 1.2
–1.5 to 3.8
Normalized Scores
low high
Deviation Scores
low high

Figure 5. scATAC-seq revealed potential transcriptional regulators in taste bud cells

Transcription factor motif analyses in accessible peaks from control mice.

(A) A heatmap of enriched motifs of transcription factors across cell clusters.

(B) DNA footprints of Trp63 and Pou5f1 across cell clusters revealed by ArchR.

(C) Correlations between gene scores of transcription factors (TF) and their motif enrichment in cell clusters. Red indicates transcription factors with significant positive correlation, suggesting they likely act as transcription activators.

(D) Side-by-side comparisons of gene scores and motif enrichment of seven transcription factors. A lack of correlation between gene score and motif enrichment suggests the transcription factor may function as transcription repressor.

Together, our results revealed strong cell-type-selective chromatin accessibility for *Tas2rs* and genes of other receptor/signaling proteins involved in taste reception and signaling. The scATAC-seq dataset can be used to identify putative *cis*-regulatory elements for taste-cell-specific gene expression, an understudied area of taste biology.

Motif analyses identified potential transcriptional regulators in taste cells

An advantage of scATAC-seq is the ability to identify candidate transcriptional regulators. To do this, we performed binding motif enrichment analysis for transcription factors using accessible peaks (Figure S6A). This analysis identified many enriched motifs for an array of transcription factors (Figure 5A and Table S4). Notably, the binding motif for Trp63 was highly enriched in the C3 and C4 cell clusters (Figures 5A and S6F). This result is highly in line with previous reports that showed Trp63 is a marker for lingual epithelial stem/progenitor cells that give rise to both taste bud cells and nontaste epithelial cells,[52,53] and that Trp63-deficient mice exhibit abnormal differentiation of the tongue epithelium.[54] Trp63 footprint analysis using ArchR also showed enrichment in C3, C4, and C7 cell clusters (Figure 5B). In addition, we identified several potential transcriptional regulators whose motifs were enriched in the C7 cluster of stem/progenitor cells, including Stat3, Tcfcp2l1 (i.e., Tfcp2l1), Nfia, and Nfib (Figure 5A). All of these transcription factors are known to play critical roles in governing stemness or other properties of stem cells.[55–57]

Furthermore, we identified multiple potential regulators of taste bud cell differentiation and/or function (Figure 5A). For instance, our results showed that the motifs of Ascl1, Ascl2, and Myod1 are enriched in type III taste bud cells (Figures 5A and S6F). Of these transcription factors, Ascl1 has been shown to play key roles in type III taste cell differentiation,[58] whereas the functions of Ascl2 and Myod1 in type III taste cells remain to be determined. The motifs of Lin54, Pou5f1, Ctcf (CCCTC-binding factor), Ctcfl (Ctcf-like), and Pit1 (Pou1f1) were enriched in type II taste cells (Figures 5A and S6F). Of these transcription factors, Ctcf was shown to play a role in the expression of human *TAS2R8*.[59] DNA footprints showed that Pou5f1, Lin54, and Pit1 are promising candidates as transcriptional regulators of type II taste cell (Figures 5B, S6B, and S6C). Similarly, the motifs of multiple transcription factors are enriched in type I taste cells (Figure 5A). Of these transcription factors, Foxa1 was reported as a potential target gene of Sonic hedgehog (Shh),[60] whose gene score was enriched in type I taste cells (Table S3). The binding motif of Sox2 was also enriched in type I cells (Figure S6F and Table S4). In addition, some of the identified transcription factors showed enriched motifs in all three taste cell clusters, such as Snai2, Tcf3, Id3, and Id4 (Figures 5A and S6F), suggesting they may play general roles in taste bud differentiation.

Transcription activators often show positive correlation between motif enrichment and gene expression, whereas transcription repressors often lack such correlation or show anti-correlation.[23,47] Next, we performed correlation analysis of gene scores (proxies for gene expression) versus motif enrichment of transcription factors. Figure 5C shows the identified potential transcription activators. Trp63, Ascl1, and Nfib are among these factors, suggesting they may act as transcription activators in taste/lingual epithelium differentiation. Figures 5D and S6G show side-by-side comparisons of gene scores and motif enrichments of various transcription factors. Notably, some of the transcription factors that have been shown to play important roles in taste cell differentiation, such as Pou2f3 and Nkx2.2, did not show correlation of gene score and motif enrichment, suggesting they may function as transcription repressors. This result is in agreement with a previous report that showed gene knockout of Pou2f3 resulted in expanded expression of type III cell-specific genes in type II taste cells,[31] suggesting Pou2f3 is a repressor of type III gene expression in type II taste cells (in addition to other possible functions). Together, our results revealed many potential transcriptional regulators in specific taste cell types.

LPS induced broad epigenetic changes in taste tissue stem cells and taste bud cells

Next, we compared the scATAC-seq datasets from PBS- and LPS-treated mice. Figure 6A shows UMAP plots of the combined dataset. The percentages of cells and accessible peaks in each cell cluster are shown in Figure 6B and Table S1. LPS treatment decreased the percentage of cells in the C7 cell cluster (11.36% in PBS vs. 8.09% in LPS dataset) but increased the percentage of cells in the C8 cell cluster (0.18% in PBS vs. 4.44% in LPS dataset). These results indicate that LPS strongly affects taste tissue stem/progenitor cells, consistent with our previous report.[21]

Gene score analysis showed many up- and down-regulated genes by LPS treatment. In particular, type I taste cells showed numerous up- and down-regulated genes (Figure 6C). Pathway analysis of up-regulated genes revealed that many immune response pathways were significantly enriched, such as the TLR signaling pathways, cytokine production and signaling pathways, MAP kinase pathways, chemokine production, and immune cell migration pathways (Figure S7A). Consistently, motif analysis showed that LPS increased the accessible motifs for nuclear factor-κB (Nfkb1 and Rel; Figure 6F), a master regulator of immune responses. These results strongly suggest that, in the presence of PAMPs, taste bud cells are capable of producing immune regulatory factors, such as cytokines and chemokines, consistent with our previous findings.[16]

Furthermore, the C3 and C7 stem/progenitor cell clusters also showed strong responses to LPS. We observed a large number of up- and down-regulated genes in these clusters (Figures 6D and 6E). LPS significantly increased the accessible binding motifs for Smarcc1 (a subunit for the chromatin remodeling complex SWI/SNF), Bach1, Bach2, Fos, and JunD (subunits of AP-1 transcription factor known to be involved in LPS-induced gene expression) (Figures 6G and 6H). These results suggest that LPS treatment induces large-scale chromatin remodeling in taste stem/progenitor cells. Pathway enrichment analysis showed up-regulation of defense pathways to LPS and bacteria, cytokine production and signaling, chemokine signaling and chemotaxis, MAP kinase cascade, and angiogenesis pathways – all related to inflammation (Figure S7B).

Of interest, we observed some differences in pathway enrichment between the C3 and C7 clusters. TNF production, response to TNF, chemotaxis, and protein translation are more enriched in the C3 cluster, whereas interferon-γ production, response to IL-1, antiviral pathways, and glucuronidation pathways are more enriched in the C7 cluster (Figure S7B). The significance of these differences remains to be determined.

LPS increased chromatin accessibility at *Tas2r* genomic loci that contain NF-κB binding sites

Next we performed detailed analysis of *Tas2r* genomic regions to evaluate whether LPS stimulation increased chromatin accessibility in these regions. As shown in Figure 2D, the expression of multiple *Tas2rs* in the genomic region between *Tas2r115* and *Tas2r125* on mouse chromosome 6 was induced >3-fold by LPS. Thus, we specifically compared the number of accessible peaks in this region between the PBS and LPS datasets. Figure 7A shows that the number of accessible peaks in this region in the LPS dataset was more than double that in the PBS dataset. Analysis of more mouse *Tas2rs* showed a general increase in the number of accessible peaks (Figure 7B). We also compared normalized peak signals in the genomic region between *Tas2r121* and *Tas2r125* from PBS- and LPS-treated mice. LPS increased chromatin accessibility at the promoter and TSS of multiple *Tas2rs* (Figures 7C and 7D). Increased accessibility to some intergenic regions within the *Tas2r* clusters were also observed.

NF-κB is a major transcription factor involved in inflammation-stimulated gene expression.[19] Previously we showed that NF-κB is expressed in taste bud cells and induced by LPS.[61] Next we investigated whether NF-κB is involved in LPS-stimulated *Tas2r* gene expression. To do this we first performed transcription factor binding site analysis of two LPS-induced *Tas2rs*, *Tas2r102* and *Tas2r116*, using PROMO, a tool for transcription factor binding site prediction.[62] PROMO identified several putative NF-κB binding sites in the promoter regions of both *Tas2r102* and *Tas2r116* (Figure 7F). These promoter regions showed increased chromatin accessibility after LPS treatment (Figures 7C and 7D). To verify whether NF-κB can bind to the promoter regions of the *Tas2rs*, we conducted chromatin immunoprecipitation (ChIP) with qPCR experiment using an antibody to NF-κB p65. To overcome the limited availability of taste buds per mouse, we used cultured taste organoids.[63] qPCR primers were selected around the putative NF-κB binding sites identified by PROMO. As a control, we also analyzed NF-κB binding to the promoter region of *Tnf*, an

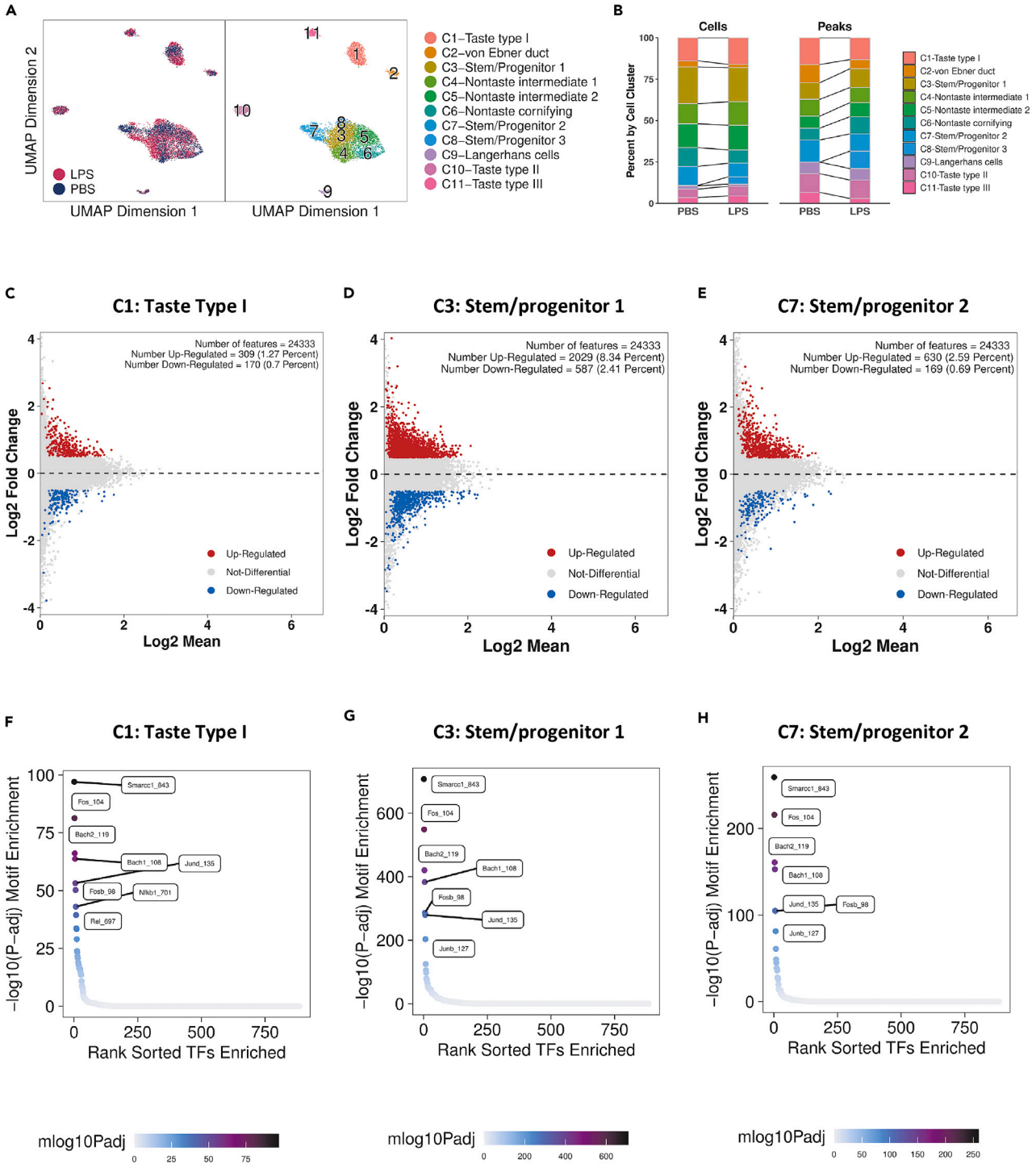

Figure 6. LPS induced broad epigenomic changes in taste bud cells and taste tissue stem/progenitor cells

(A) UMAP plots. Left: Comparison of cells from control (PBS) and LPS-treated mice. Right: Cell clusters in the PBS and LPS combined dataset.

(B) Percentages of cells and accessible peaks in each cell cluster. LPS treatment resulted in changes in the proportion of cells and peaks in some cell clusters.

(C–E) Up- and down-regulated genes (based on gene scores) in type I taste cells (C) and two clusters of taste tissue stem/progenitor cells (D and E).

(F–H) Up-regulated transcription factor (TF) motifs by LPS in type I taste cells (F) and two clusters of taste tissue stem/progenitor cells (G and H).

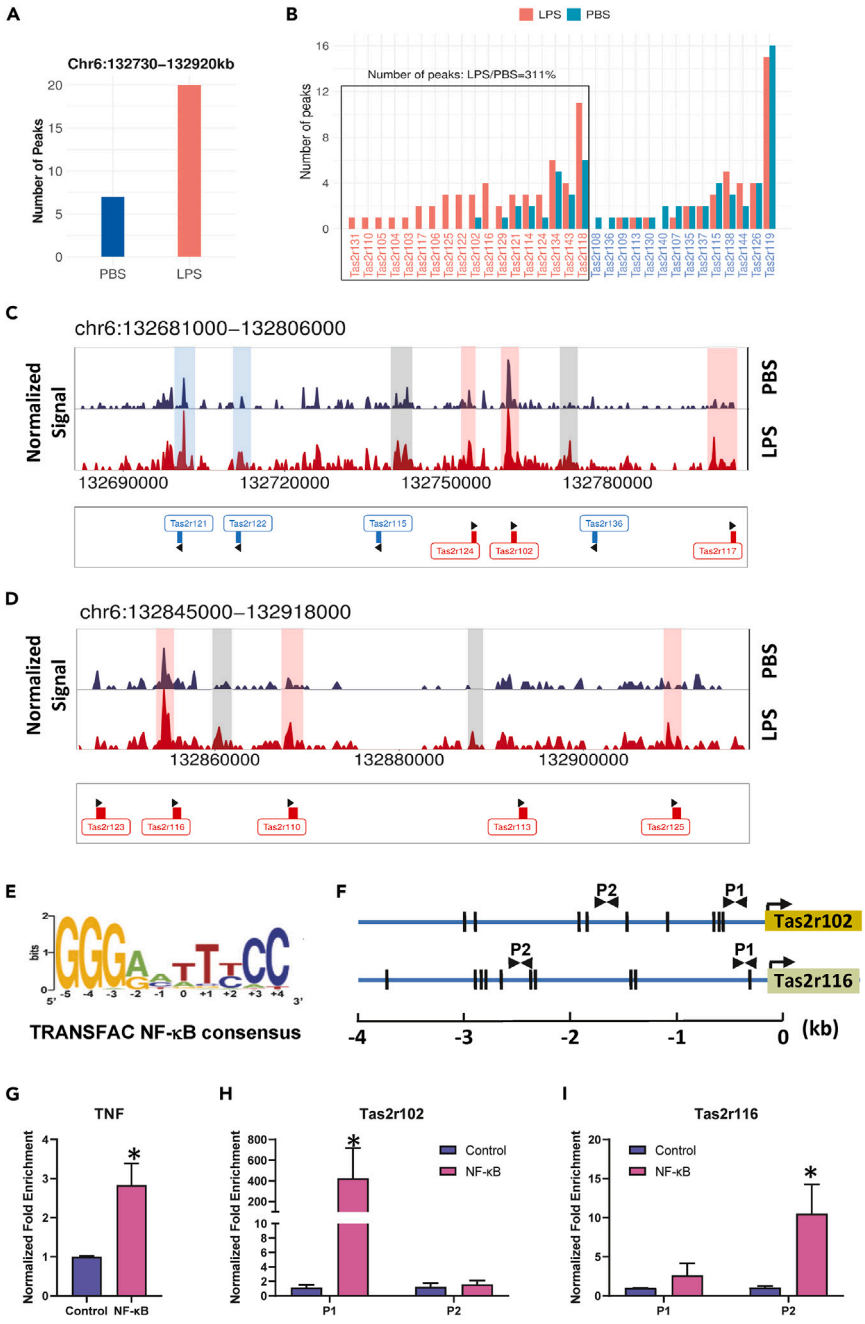

Figure 7. LPS increased chromatin accessibility at *Tas2r* genomic loci that contain NF-κB binding sites

Comparison of chromatin accessibility of the *Tas2r* loci between PBS- (control) and LPS-treated mice.

(A) Number of accessible peaks in the genomic region of the *Tas2r* gene cluster between *Tas2r115* and *Tas2r125* on chromosome 6 that harbors several LPS-highly inducible *Tas2rs*. LPS treatment markedly increased the number of peaks in this region.

(B) Number of accessible peaks for individual *Tas2rs*. LPS increased the number of peaks for the majority of *Tas2rs* (boxed area).

(C and D) Comparison of normalized peaks between the PBS and LPS groups in two *Tas2r* regions on chromosome 6. Gene symbols in red indicate genes transcribed in the forward direction, and their LPS-induced accessible peaks are highlighted in pink. Gene symbols in blue indicate genes transcribed in the reverse direction, and their LPS-induced accessible peaks are highlighted in blue. Gray bars highlight LPS-inducible peaks in intergenic regions. Black arrowheads indicate direction of *Tas2r* gene transcription.

(E) NF-κB consensus binding site in the TRANSFAC database.

Figure 7. *Continued*

(F) Putative NF-κB binding sites (indicated by vertical black bars) identified using PROMO in 4 kb regions around TTS of *Tas2r102* and *Tas2r116*.

(G–I) ChIP-qPCR analysis of NF-κB binding to the promoter regions of *Tnf* (G), *Tas2r102* (H), and *Tas2r116* (I). Chromatin immunoprecipitations were performed with cross-linked chromatin from cultured taste organoids treated with LPS for 72 h. An antibody specific for NF-κB or a normal nonspecific rabbit IgG (Control) was used. The qPCR amplified *Tas2r* genomic regions are shown in (F). Fold enrichment was normalized to the control antibody. Data are means ± SEM. *p<0.05.

NF-κB regulated gene[64,65] that is also expressed in taste bud cells.[66] ChIP-qPCR experiments revealed enriched NF-κB pull-down signals in the promoter regions of *Tnf*, *Tas2r102*, and *Tas2r116* (Figures 7G–7I), suggesting binding of NF-κB to these regions. The pull-down signals were particularly enriched in the promoter regions with two or more putative NF-κB binding sites (Figures 7F, 7H, and 7I).

Together, our results suggest that LPS increases chromatin accessibility of many *Tas2rs*, which may allow binding of inflammation-activated transcription factors, such as NF-κB, to the regulatory regions of *Tas2rs* to stimulate gene expression.

DISCUSSION

In this study we showed that inflammation induced by LPS augmented bitter taste via epigenetic mechanisms that increased *Tas2r* gene expression. scATAC-seq identified many potential *cis*-regulatory regions in *Tas2rs* and other taste signaling genes and candidate transcriptional regulators in taste bud cells. We also observed extensive responses in taste stem/progenitor cells and type I taste cells to LPS stimulation. Our study identified a previously unrecognized mechanism for modulating *Tas2r* gene expression and bitter taste.

Recent research has shown that taste GPCRs play important roles not only in the taste system but also in many extraoral tissues.[4] T2Rs in solitary chemosensory cells are involved in detecting bacterial quorum-sensing molecules and triggering antimicrobial responses.[2,3] LPS-induced *Tas2r* expression in taste buds could be part of the general immune response to a pathogen-derived molecule. Increased sensitivity to bitter compounds may enhance antimicrobial defense and alert the host to avoid exposure to toxins. The LPS-induced hyper-responsiveness to bitter compounds is consistent with our previous findings that showed knockout of TNF, a key inflammatory cytokine expressed by many immune cells as well as by taste bud cells, resulted in specific reduction in neural and behavioral responses to bitter compounds.[67] Together, our studies provide strong evidence that bitter taste is selectively regulated by immune factors at the peripheral level.

Taste dysfunction contributes to loss of appetite. Elevated bitter taste could be a part of the anorexic responses associated with systemic inflammation. This mechanism may also contribute to rejection of bitter medicine, especially in young children. In this case, masking or down-regulating bitter taste could be beneficial. It is well established that LPS treatment reduces preference and intake of sweet taste compounds,[22] which is considered a behavioral change related to depression caused by sickness.[68] Inflammatory cytokines, such as TNF and IL-1β, may play important roles in such behavioral changes by acting on various brain regions.[68] Our behavioral and nerve recording results with sweet taste compounds (Figures 1 and S1) support these proposed brain mechanisms. Moreover, an intriguing recent study showed that fasting was protective in bacterial sepsis,[69] suggesting anorexia may have important physiological roles during bacterial infections.

LPS-induced gene expression in macrophages can be separated into stages. Early primary response genes are induced quickly and do not require new protein synthesis, whereas secondary response genes are induced at a later time and largely depend on new protein synthesis and chromatin remodeling for induction.[19,70] *Tas2rs* are likely secondary or even tertiary response genes because of their delayed induction (Figure 2). Our results show that the LPS-induced expression of *Tas2rs* in the taste epithelium peaks around 3–5 days after LPS treatment and mostly returns to the basal levels on day 10 (Figures 2B and 2C). This time course is consistent with late response genes. In line with this, chromatin accessibility of the majority of *Tas2rs* is increased by LPS (Figures 7A–7D), indicating remodeling of nucleosomes at *Tas2r* loci. In addition, we found that the regulatory regions of some Tas2rs contain NF-κB binding sites (Figures 7F, 7H, and 7I). In the canonical TLR4 signaling pathways, binding of LPS to TLR4 leads to NF-κB activation and nuclear

translocation. This process occurs within a few hours of LPS stimulation in macrophages,[19] but its time course in taste cells is unknown. TNF, an LPS stimulated inflammatory cytokine, is another inducer of NF-κB activation. Previously, we showed that in taste tissues TNF production induced by LPS can last for more than 2 days,[61,66] much longer than that in macrophages. It is possible that the LPS-induced *Tas2r* gene expression involves both direct activation by TLR4 pathways and indirect activation by cytokine pathways (e.g., TNF signaling pathways). Of interest, COVID-19 infection also induces widespread changes in olfactory receptor gene expression,[71] another example of large-scale change in chemosensory receptor expression as an underlying cause for sensory dysfunction.

Emerging evidence shows that tissue stem cells play important regulatory roles in immune responses.[72,73] Stem cells not only can produce cytokines and chemokines[72] but also can harbor epigenetic memory, which allows them to respond faster to future stimulation.[73] Such immune memory is advantageous against future infections but may also contribute to chronic diseases. We observed that taste tissue stem/progenitor cells showed robust epigenetic responses to LPS treatment (Figure 6), with up-regulation of numerous pathways related to cytokine/chemokine production and inflammation (Figure S7). The motifs of Smarcc1, a subunit of the chromatin remodeling complex SWI/SNF, were dramatically enriched in stem/progenitor cells after LPS induction, suggesting Smarcc1 may play key roles in LPS-induced chromatin remodeling in taste stem/progenitor cells. It is conceivable that chromatin remodeling may result in "inflammatory memory" in taste tissue stem/progenitor cells, leading to long-lasting effects on taste responses.

Our study identified many potential cell-type-selective transcriptional regulators (Figure 5). Transcriptional regulation of taste receptors and signaling proteins remains poorly understood. Only a handful of transcription factors have been shown to play roles in taste cell differentiation. Consistent with previous publications, our results show that the motifs and gene scores of Trp63 and Ascl1 are enriched in taste stem/progenitor cells and type III taste bud cells, respectively (Figure 5D). Their binding motifs and gene scores are highly correlated (Figure 5C), suggesting they are transcription activators. Conversely, Pou2f3, Pou5f1, and Pou1f1 did not show correlation between enrichment of gene scores and that of their binding motifs, suggesting they may act as transcription repressors. The phenotype of Pou2f3-knockout mice supports this proposition: lacking Pou2f3 results in expression of type III cell-specific genes in type II taste cells.[31] Further characterization of these transcription factors and identification of their downstream targets can help determine their roles in taste bud cell differentiation as well as in taste alterations associated with diseases.

Limitations of the study

Our study provides a molecular mechanism for LPS-induced bitter taste response. scATAC-seq revealed epigenetic changes at the *Tas2r* loci after LPS treatments that correlate with the increased *Tas2r* gene expression and heightened bitter taste response. This study also identified putative transcription factors and *cis*-regulatory motifs for controlling the expression of taste receptors and signaling proteins. Although scATAC-seq is a powerful tool for studying gene regulation, the regulatory factors and motifs identified by the method need to be further investigated in future studies.

STAR★METHODS

Detailed methods are provided in the online version of this paper and include the following:

- KEY RESOURCES TABLE
- RESOURCE AVAILABILITY
  - Lead contact
  - Materials availability
  - Data and code availability
- EXPERIMENTAL MODEL AND SUBJECT DETAILS
  - Animals
  - Taste organoid culture
- METHOD DETAILS
  - Brief-access behavioral tests
  - Gustatory nerve recordings
  - qRT-PCR
  - Isolation of nuclei, preparation of scATAC-seq libraries, and high-throughput sequencing

- Data processing with Cell Ranger ATAC pipeline
- Data analyses with the ArchR pipeline
- Pathway enrichment analysis
- ChIP-qPCR experiment

- QUANTIFICATION AND STATISTICAL ANALYSIS

SUPPLEMENTAL INFORMATION

Supplemental information can be found online at https://doi.org/10.1016/j.isci.2023.106920.

ACKNOWLEDGMENTS

This study was supported in part by National Institutes of Health/National Institute of Deafness and Other Communication Disorders (NIH/NIDCD) grants R01DC018042 (H.W.), R01DC018042-02S1 (H.W.), R42DC017693 (D.R.R.), and P30 DC011735 (R.F.M.). We also acknowledge funding from NIH G20OD020296 (D.R.R.; an infrastructure improvement grant at the Monell Chemical Senses Center). The graphical abstract was created with BioRender.com.

AUTHOR CONTRIBUTIONS

C.L., M.J., J.Q., S.F., M.Z., and H.W. performed the experiments and analyzed the results. L.H. provided PCR primers for *Tas2rs*. Y.N., R.F.M., D.R.R., and H.W. co-supervised nerve recording experiments and/or scATAC-seq data analyses. All authors were involved in data discussion and results interpretation. C.L., P.J., I.M., L.H., R.F.M., D.R.R., and H.W. were involved in drafting or editing the manuscript.

DECLARATION OF INTERESTS

The authors declare no competing interests.

INCLUSION AND DIVERSITY

We support inclusive, diverse, and equitable conduct of research.

Received: August 4, 2022
Revised: February 27, 2023
Accepted: May 15, 2023
Published: May 19, 2023

REFERENCES

1. Adler, E., Hoon, M.A., Mueller, K.L., Chandrashekar, J., Ryba, N.J., and Zuker, C.S. (2000). A novel family of mammalian taste receptors. Cell *100*, 693–702.

2. Tizzano, M., Gulbransen, B.D., Vandenbeuch, A., Clapp, T.R., Herman, J.P., Sibhatu, H.M., Churchill, M.E.A., Silver, W.L., Kinnamon, S.C., and Finger, T.E. (2010). Nasal chemosensory cells use bitter taste signaling to detect irritants and bacterial signals. Proc. Natl. Acad. Sci. USA *107*, 3210–3215. https://doi.org/10.1073/pnas.0911934107.

3. Lee, R.J., Kofonow, J.M., Rosen, P.L., Siebert, A.P., Chen, B., Doghramji, L., Xiong, G., Adappa, N.D., Palmer, J.N., Kennedy, D.W., et al. (2014). Bitter and sweet taste receptors regulate human upper respiratory innate immunity. J. Clin. Invest. *124*, 1393–1405. https://doi.org/10.1172/JCI72094.

4. Wang, H., Matsumoto, I., and Jiang, P. (2022). Immune regulatory roles of cells expressing taste signaling elements in nongustatory tissues. Handb. Exp. Pharmacol. *275*, 271–293. https://doi.org/10.1007/164_2021_468.

5. Luo, X.C., Chen, Z.H., Xue, J.B., Zhao, D.X., Lu, C., Li, Y.H., Li, S.M., Du, Y.W., Liu, Q., Wang, P., et al. (2019). Infection by the parasitic helminth Trichinella spiralis activates a Tas2r-mediated signaling pathway in intestinal tuft cells. Proc. Natl. Acad. Sci. USA *116*, 5564–5569. https://doi.org/10.1073/pnas.1812901116.

6. Miller, C.N., Proekt, I., von Moltke, J., Wells, K.L., Rajpurkar, A.R., Wang, H., Rattay, K., Khan, I.S., Metzger, T.C., Pollack, J.L., et al. (2018). Thymic tuft cells promote an IL-4-enriched medulla and shape thymocyte development. Nature *559*, 627–631. https://doi.org/10.1038/s41586-018-0345-2.

7. Grassin-Delyle, S., Naline, E., and Devillier, P. (2015). Taste receptors in asthma. Curr.Opin.Allergy Clin.Immunol. *15*, 63–69. https://doi.org/10.1097/ACI.0000000000000137.

8. Cowart, B.J. (2005). Taste, our body's gustatory gatekeeper. Cerebrum *7*, 7–22. http://www.dana.org/news/cerebrum/detail.aspx?id=788.

9. Hayes, J.E., Wallace, M.R., Knopik, V.S., Herbstman, D.M., Bartoshuk, L.M., and Duffy, V.B. (2011). Allelic variation in TAS2R bitter receptor genes associates with variation in sensations from and ingestive behaviors toward common bitter beverages in adults. Chem. Senses *36*, 311–319. https://doi.org/10.1093/chemse/bjq132.

10. Duffy, V.B., Hayes, J.E., Davidson, A.C., Kidd, J.R., Kidd, K.K., and Bartoshuk, L.M. (2010). Vegetable intake in college-aged adults is explained by oral sensory phenotypes and TAS2R38 genotype. Chemosens.Percept. *3*, 137–148. https://doi.org/10.1007/s12078-010-9079-8.

11. Hinrichs, A.L., Wang, J.C., Bufe, B., Kwon, J.M., Budde, J., Allen, R., Bertelsen, S., Evans, W., Dick, D., Rice, J., et al. (2006). Functional variant in a bitter-taste receptor (hTAS2R16) influences risk of alcohol dependence. Am. J. Hum. Genet. *78*, 103–111. https://doi.org/10.1086/499253.

12. Drayna, D. (2005). Human taste genetics. Annu. Rev. Genom. Hum. Genet. *6*, 217–235.

https://doi.org/10.1146/annurev.genom.6.080604.162340.

13. Schiffman, S.S. (1983). Taste and smell in disease (first of two parts). N. Engl. J. Med. *308*, 1275–1279.

14. Thomas, D.C., Chablani, D., Parekh, S., Pichammal, R.C., Shanmugasundaram, K., and Pitchumani, P.K. (2022). Dysgeusia: a review in the context of COVID-19. J. Am. Dent. Assoc. *153*, 251–264. https://doi.org/10.1016/j.adaj.2021.08.009.

15. Doyle, M.E., Appleton, A., Liu, Q.R., Yao, Q., Mazucanti, C.H., and Egan, J.M. (2021). Human type II taste cells express angiotensin-converting enzyme 2 and are infected by severe acute respiratory syndrome coronavirus 2 (SARS-CoV-2). Am. J. Pathol. *191*, 1511–1519. https://doi.org/10.1016/j.ajpath.2021.05.010.

16. Wang, H., Zhou, M., Brand, J., and Huang, L. (2007). Inflammation activates the interferon signaling pathways in taste bud cells. J. Neurosci. *27*, 10703–10713.

17. Wang, H., Zhou, M., Brand, J., and Huang, L. (2009). Inflammation and taste disorders: mechanisms in taste buds. Ann. N. Y. Acad. Sci. *1170*, 596–603.

18. Qin, Y., Palayyan, S.R., Zheng, X., Tian, S., Margolskee, R.F., and Sukumaran, S.K. (2023). Type II taste cells participate in mucosal immune surveillance. PLoS Biol. *21*, e3001647. https://doi.org/10.1371/journal.pbio.3001647.

19. Medzhitov, R., and Horng, T. (2009). Transcriptional control of the inflammatory response. Nat. Rev. Immunol. *9*, 692–703. https://doi.org/10.1038/nri2634.

20. Janeway, C.A., Jr., and Medzhitov, R. (1999). Lipoproteins take their toll on the host. Curr.Biol. *9*, R879–R882. https://doi.org/10.1016/s0960-9822(00)80073-1.

21. Cohn, Z.J., Kim, A., Huang, L., Brand, J., and Wang, H. (2010). Lipopolysaccharide-induced inflammation attenuates taste progenitor cell proliferation and shortens the life span of taste bud cells. BMC Neurosci. *11*, 72.

22. Dantzer, R. (2001). Cytokine-induced sickness behavior: mechanisms and implications. Ann. N. Y. Acad. Sci. *933*, 222–234.

23. Granja, J.M., Corces, M.R., Pierce, S.E., Bagdatli, S.T., Choudhry, H., Chang, H.Y., and Greenleaf, W.J. (2021). ArchR is a scalable software package for integrative single-cell chromatin accessibility analysis. Nat. Genet. *53*, 403–411. https://doi.org/10.1038/s41588-021-00790-6.

24. Ziffra, R.S., Kim, C.N., Ross, J.M., Wilfert, A., Turner, T.N., Haeussler, M., Casella, A.M., Przytycki, P.F., Keough, K.C., Shin, D., et al. (2021). Single-cell epigenomics reveals mechanisms of human cortical development. Nature *598*, 205–213. https://doi.org/10.1038/s41586-021-03209-8.

25. Finger, T.E. (2005). Cell types and lineages in taste buds. Chem. Senses *30* (*Suppl 1*), i54–i55.

26. Roper, S.D., and Chaudhari, N. (2017). Taste buds: cells, signals and synapses. Nat. Rev. Neurosci. *18*, 485–497. https://doi.org/10.1038/nrn.2017.68.

27. Dvoryanchikov, G., Sinclair, M.S., Perea-Martinez, I., Wang, T., and Chaudhari, N. (2009). Inward rectifier channel, ROMK, is localized to the apical tips of glial-like cells in mouse taste buds. J. Comp. Neurol. *517*, 1–14. https://doi.org/10.1002/cne.22152.

28. Bartel, D.L., Sullivan, S.L., Lavoie, E.G., Sévigny, J., and Finger, T.E. (2006). Nucleoside triphosphate diphosphohydrolase-2 is the ecto-ATPase of type I cells in taste buds. J. Comp. Neurol. *497*, 1–12.

29. Rodriguez, Y.A., Roebber, J.K., Dvoryanchikov, G., Makhoul, V., Roper, S.D., and Chaudhari, N. (2021). "Tripartite synapses" in taste buds: arole for type I glial-like taste cells. J. Neurosci. *41*, 9860–9871. https://doi.org/10.1523/JNEUROSCI.1444-21.2021.

30. Chandrashekar, J., Yarmolinsky, D., von Buchholtz, L., Oka, Y., Sly, W., Ryba, N.J.P., and Zuker, C.S. (2009). The taste of carbonation. Science *326*, 443–445. https://doi.org/10.1126/science.1174601.

31. Matsumoto, I., Ohmoto, M., Narukawa, M., Yoshihara, Y., and Abe, K. (2011). Skn-1a (Pou2f3) specifies taste receptor cell lineage. Nat. Neurosci. *14*, 685–687.

32. Ogata, T., and Ohtubo, Y. (2020). Quantitative analysis of taste bud cell numbers in the circumvallate and foliate taste buds of mice. Chem. Senses *45*, 261–273. https://doi.org/10.1093/chemse/bjaa017.

33. Hauser, B.R., Aure, M.H., Kelly, M.C., Genomics Computational Biology, C., Hoffman, M.P., and Chibly, A.M. (2020). Generation of a single-cell RNAseq atlas of murine salivary gland development. iScience *23*, 101838. https://doi.org/10.1016/j.isci.2020.101838.

34. Li, X.J., and Snyder, S.H. (1995). Molecular cloning of Ebnerin, a von Ebner's gland protein associated with taste buds. J. Biol. Chem. *270*, 17674–17679. https://doi.org/10.1074/jbc.270.30.17674.

35. Asano-Miyoshi, M., Kusakabe, Y., Abe, K., and Emori, Y. (1998). Identification of taste-tissue-specific cDNA clones from a subtraction cDNA library of rat circumvallate and foliate papillae. J. Biochem. *124*, 927–933. https://doi.org/10.1093/oxfordjournals.jbchem.a022209.

36. Doebel, T., Voisin, B., and Nagao, K. (2017). Langerhans cells - the macrophage in dendritic cell clothing. Trends Immunol. *38*, 817–828. https://doi.org/10.1016/j.it.2017.06.008.

37. Muskhelishvili, L., Latendresse, J.R., Kodell, R.L., and Henderson, E.B. (2003). Evaluation of cell proliferation in rat tissues with BrdU, PCNA, Ki-67(MIB-5) immunohistochemistry and in situ hybridization for histone mRNA. J. Histochem. Cytochem. *51*, 1681–1688. https://doi.org/10.1177/002215540305101212.

38. Bologna-Molina, R., Mosqueda-Taylor, A., Molina-Frechero, N., Mori-Estevez, A.D., and Sánchez-Acuña, G. (2013). Comparison of the value of PCNA and Ki-67 as markers of cell proliferation in ameloblastic tumors. Med. Oral Patol.Oral Cir. Bucal *18*, e174–e179. https://doi.org/10.4317/medoral.18573.

39. Shelton, J.F., Shastri, A.J., Fletez-Brant, K., 23andMe COVID-19 Team, Aslibekyan, S., and Auton, A. (2022). The UGT2A1/UGT2A2 locus is associated with COVID-19-related loss of smell or taste. Nat. Genet. *54*, 121–124. https://doi.org/10.1038/s41588-021-00986-w.

40. Eckhart, L., Lippens, S., Tschachler, E., and Declercq, W. (2013). Cell death by cornification. Biochim.Biophys. Acta *1833*, 3471–3480. https://doi.org/10.1016/j.bbamcr.2013.06.010.

41. Miura, H., Kusakabe, Y., Hashido, K., Hino, A., Ooki, M., and Harada, S. (2014). The glossopharyngeal nerve controls epithelial expression of Sprr2a and Krt13 around taste buds in the circumvallate papilla. Neurosci.Lett. *580*, 147–152. https://doi.org/10.1016/j.neulet.2014.08.012.

42. Fuchs, E., and Raghavan, S. (2002). Getting under the skin of epidermal morphogenesis. Nat. Rev. Genet. *3*, 199–209. https://doi.org/10.1038/nrg758.

43. Reimand, J., Arak, T., Adler, P., Kolberg, L., Reisberg, S., Peterson, H., and Vilo, J. (2016). g:Profiler-a web server for functional interpretation of gene lists (2016 update). Nucleic Acids Res. *44*, W83–W89. https://doi.org/10.1093/nar/gkw199.

44. Raudvere, U., Kolberg, L., Kuzmin, I., Arak, T., Adler, P., Peterson, H., and Vilo, J. (2019). g:Profiler: a web server for functional enrichment analysis and conversions of gene lists (2019 update). Nucleic Acids Res. *47*, W191–W198. https://doi.org/10.1093/nar/gkz369.

45. Shannon, P., Markiel, A., Ozier, O., Baliga, N.S., Wang, J.T., Ramage, D., Amin, N., Schwikowski, B., and Ideker, T. (2003). Cytoscape: a software environment for integrated models of biomolecular interaction networks. Genome Res. *13*, 2498–2504. https://doi.org/10.1101/gr.1239303.

46. Merico, D., Isserlin, R., Stueker, O., Emili, A., and Bader, G.D. (2010). Enrichment map: a network-based method for gene-set enrichment visualization and interpretation. PLoS One *5*, e13984. https://doi.org/10.1371/journal.pone.0013984.

47. Finkbeiner, C., Ortuño-Lizarán, I., Sridhar, A., Hooper, M., Petter, S., and Reh, T.A. (2022).

Single-cell ATAC-seq of fetal human retina and stem-cell-derived retinal organoids shows changing chromatin landscapes during cell fate acquisition. Cell Rep. *38*, 110294. https://doi.org/10.1016/j.celrep.2021.110294.

48. Pérez, C.A., Huang, L., Rong, M., Kozak, J.A., Preuss, A.K., Zhang, H., Max, M., and Margolskee, R.F. (2002). A transient receptor potential channel expressed in taste receptor cells. Nat. Neurosci. *5*, 1169–1176.

49. Ohmoto, M., Matsumoto, I., Misaka, T., and Abe, K. (2006). Taste receptor cells express voltage-dependent potassium channels in a cell age-specific manner. Chem. Senses *31*, 739–746. https://doi.org/10.1093/chemse/bjl016.

50. Wang, H., Iguchi, N., Rong, Q., Zhou, M., Ogunkorode, M., Inoue, M., Pribitkin, E.A., Bachmanov, A.A., Margolskee, R.F., Pfeifer, K., and Huang, L. (2009). Expression of the voltage-gated potassium channel KCNQ1 in mammalian taste bud cells and the effect of its null-mutation on taste preferences. J. Comp. Neurol. *512*, 384–398.

51. Teng, B., Wilson, C.E., Tu, Y.H., Joshi, N.R., Kinnamon, S.C., and Liman, E.R. (2019). Cellular and neural responses to sour stimuli require the proton channel Otop1. Curr.Biol. *29*, 3647–3656.e5. https://doi.org/10.1016/j.cub.2019.08.077.

52. Okubo, T., Clark, C., and Hogan, B.L.M. (2009). Cell lineage mapping of taste bud cells and keratinocytes in the mouse tongue and soft palate. Stem Cell. *27*, 442–450.

53. Bloomquist, R.F., Fowler, T.E., An, Z., Yu, T.Y., Abdilleh, K., Fraser, G.J., Sharpe, P.T., and Streelman, J.T. (2019). Developmental plasticity of epithelial stem cells in tooth and taste bud renewal. Proc. Natl. Acad. Sci. USA *116*, 17858–17866. https://doi.org/10.1073/pnas.1821202116.

54. Mills, A.A., Zheng, B., Wang, X.J., Vogel, H., Roop, D.R., and Bradley, A. (1999). p63 is a p53 homologue required for limb and epidermal morphogenesis. Nature *398*, 708–713. https://doi.org/10.1038/19531.

55. Raz, R., Lee, C.K., Cannizzaro, L.A., d'Eustachio, P., and Levy, D.E. (1999). Essential role of STAT3 for embryonic stem cell pluripotency. Proc. Natl. Acad. Sci. USA *96*, 2846–2851. https://doi.org/10.1073/pnas.96.6.2846.

56. Tchieu, J., Calder, E.L., Guttikonda, S.R., Gutzwiller, E.M., Aromolaran, K.A., Steinbeck, J.A., Goldstein, P.A., and Studer, L. (2019). NFIA is a gliogenic switch enabling rapid derivation of functional human astrocytes from pluripotent stem cells. Nat. Biotechnol. *37*, 267–275. https://doi.org/10.1038/s41587-019-0035-0.

57. Chang, C.Y., Pasolli, H.A., Giannopoulou, E.G., Guasch, G., Gronostajski, R.M., Elemento, O., and Fuchs, E. (2013). NFIB is a governor of epithelial-melanocyte stem cell behaviour in a shared niche. Nature *495*, 98–102. https://doi.org/10.1038/nature11847.

58. Seta, Y., Oda, M., Kataoka, S., Toyono, T., and Toyoshima, K. (2011). Mash1 is required for the differentiation of AADC-positive type III cells in mouse taste buds. Dev. Dynam. *240*, 775–784. https://doi.org/10.1002/dvdy.22576.

59. Kojima, T., Maeda, T., Suzuki, A., Yamamori, T., and Kato, Y. (2020). Intracellular zinc-dependent TAS2R8 gene expression through CTCF activation. Biomed. Res. *41*, 217–225. https://doi.org/10.2220/biomedres.41.217.

60. Golden, E.J., Larson, E.D., Shechtman, L.A., Trahan, G.D., Gaillard, D., Fellin, T.J., Scott, J.K., Jones, K.L., and Barlow, L.A. (2021). Onset of taste bud cell renewal starts at birth and coincides with a shift in SHH function. Elife *10*, e64013. https://doi.org/10.7554/eLife.64013.

61. Feng, S., Achoute, L., Margolskee, R.F., Jiang, P., and Wang, H. (2020). Lipopolysaccharide-induced inflammatory cytokine expression in taste organoids. Chem. Senses *45*, 187–194. https://doi.org/10.1093/chemse/bjaa002.

62. Messeguer, X., Escudero, R., Farré, D., Núñez, O., Martínez, J., and Albà, M.M. (2002). PROMO: detection of known transcription regulatory elements using species-tailored searches. Bioinformatics *18*, 333–334.

63. Ren, W., Lewandowski, B.C., Watson, J., Aihara, E., Iwatsuki, K., Bachmanov, A.A., Margolskee, R.F., and Jiang, P. (2014). Single Lgr5- or Lgr6-expressing taste stem/progenitor cells generate taste bud cells ex vivo. Proc. Natl. Acad. Sci. USA *111*, 16401–16406. https://doi.org/10.1073/pnas.1409064111.

64. Shakhov, A.N., Collart, M.A., Vassalli, P., Nedospasov, S.A., and Jongeneel, C.V. (1990). Kappa B-type enhancers are involved in lipopolysaccharide-mediated transcriptional activation of the tumor necrosis factor alpha gene in primary macrophages. J. Exp. Med. *171*, 35–47. https://doi.org/10.1084/jem.171.1.35.

65. Drouet, C., Shakhov, A.N., and Jongeneel, C.V. (1991). Enhancers and transcription factors controlling the inducibility of the tumor necrosis factor-alpha promoter in primary macrophages. J. Immunol. *147*, 1694–1700.

66. Feng, P., Zhao, H., Chai, J., Huang, L., and Wang, H. (2012). Expression and secretion of TNF-alpha in mouse taste buds: anovel function of a specific subset of type II taste cells. PLoS One *7*, e43140. https://doi.org/10.1371/journal.pone.0043140.

67. Feng, P., Jyotaki, M., Kim, A., Chai, J., Simon, N., Zhou, M., Bachmanov, A.A., Huang, L., and Wang, H. (2015). Regulation of bitter taste responses by tumor necrosis factor. Brain Behav. Immun. *49*, 32–42. https://doi.org/10.1016/j.bbi.2015.04.001.

68. Dantzer, R., O'Connor, J.C., Freund, G.G., Johnson, R.W., and Kelley, K.W. (2008). From inflammation to sickness and depression: when the immune system subjugates the brain. Nat. Rev. Neurosci. *9*, 46–56. https://doi.org/10.1038/nrn2297.

69. Wang, A., Huen, S.C., Luan, H.H., Yu, S., Zhang, C., Gallezot, J.D., Booth, C.J., and Medzhitov, R. (2016). Opposing effects of fasting metabolism on tissue tolerance in bacterial and viral inflammation. Cell *166*, 1512–1525.e12. https://doi.org/10.1016/j.cell.2016.07.026.

70. Ramirez-Carrozzi, V.R., Nazarian, A.A., Li, C.C., Gore, S.L., Sridharan, R., Imbalzano, A.N., and Smale, S.T. (2006). Selective and antagonistic functions of SWI/SNF and Mi-2beta nucleosome remodeling complexes during an inflammatory response. Genes Dev. *20*, 282–296. https://doi.org/10.1101/gad.1383206.

71. Zazhytska, M., Kodra, A., Hoagland, D.A., Frere, J., Fullard, J.F., Shayya, H., McArthur, N.G., Moeller, R., Uhl, S., Omer, A.D., et al. (2022). Non-cell-autonomous disruption of nuclear architecture as a potential cause of COVID-19-induced anosmia. Cell *185*, 1052–1064.e12. https://doi.org/10.1016/j.cell.2022.01.024.

72. Chen, M., Reed, R.R., and Lane, A.P. (2019). Chronic inflammation directs an olfactory stem cell functional switch from neuroregeneration to immune defense. Cell Stem Cell *25*, 501–513.e5. https://doi.org/10.1016/j.stem.2019.08.011.

73. Naik, S., Larsen, S.B., Cowley, C.J., and Fuchs, E. (2018). Two to tango: dialog between immunity and stem cells in Health and disease. Cell *175*, 908–920. https://doi.org/10.1016/j.cell.2018.08.071.

74. Xu, J., Cao, J., Iguchi, N., Riethmacher, D., and Huang, L. (2013). Functional characterization of bitter-taste receptors expressed in mammalian testis. Mol. Hum. Reprod. *19*, 17–28. https://doi.org/10.1093/molehr/gas040.

75. Gaspar, J.M. (2018). Improved peak-calling with MACS2. Preprint at bioRxiv. https://doi.org/10.1101/496521.

76. Ren, W., Aihara, E., Lei, W., Gheewala, N., Uchiyama, H., Margolskee, R.F., Iwatsuki, K., and Jiang, P. (2017). Transcriptome analyses of taste organoids reveal multiple pathways involved in taste cell generation. Sci. Rep. *7*, 4004. https://doi.org/10.1038/s41598-017-04099-5.

77. Kim, A., Feng, P., Ohkuri, T., Sauers, D., Cohn, Z.J., Chai, J., Nelson, T., Bachmanov, A.A., Huang, L., and Wang, H. (2012). Defects in the peripheral taste structure and function in the MRL/lpr mouse model of autoimmune disease. PLoS One *7*, e35588. https://doi.org/10.1371/journal.pone.0035588.

78. Li, H., and Durbin, R. (2010). Fast and accurate long-read alignment with Burrows-Wheeler transform. Bioinformatics *26*, 589–595. https://doi.org/10.1093/bioinformatics/btp698.

79. Satpathy, A.T., Granja, J.M., Yost, K.E., Qi, Y., Meschi, F., McDermott, G.P., Olsen, B.N., Mumbach, M.R., Pierce, S.E., Corces, M.R., et al. (2019). Massively parallel single-cell

chromatin landscapes of human immune cell development and intratumoral T cell exhaustion. Nat. Biotechnol. *37*, 925–936. https://doi.org/10.1038/s41587-019-0206-z.

80. Korsunsky, I., Millard, N., Fan, J., Slowikowski, K., Zhang, F., Wei, K., Baglaenko, Y., Brenner, M., Loh, P.R., and Raychaudhuri, S. (2019). Fast, sensitive and accurate integration of single-cell data with Harmony. Nat. Methods *16*, 1289–1296. https://doi.org/10.1038/s41592-019-0619-0.

81. van Dijk, D., Sharma, R., Nainys, J., Yim, K., Kathail, P., Carr, A.J., Burdziak, C., Moon, K.R., Chaffer, C.L., Pattabiraman, D., et al. (2018). Recovering gene interactions from single-cell data using data diffusion. Cell *174*, 716–729.e27. https://doi.org/10.1016/j.cell.2018.05.061.

82. Schep, A.N., Wu, B., Buenrostro, J.D., and Greenleaf, W.J. (2017). chromVAR: inferring transcription-factor-associated accessibility from single-cell epigenomic data. Nat. Methods *14*, 975–978. https://doi.org/10.1038/nmeth.4401.

83. Reimand, J., Isserlin, R., Voisin, V., Kucera, M., Tannus-Lopes, C., Rostamianfar, A., Wadi, L., Meyer, M., Wong, J., Xu, C., et al. (2019). Pathway enrichment analysis and visualization of omics data using g:Profiler, GSEA, Cytoscape and EnrichmentMap. Nat. Protoc. *14*, 482–517. https://doi.org/10.1038/s41596-018-0103-9.

STAR★METHODS

KEY RESOURCES TABLE

REAGENT or RESOURCE	SOURCE	IDENTIFIER
Antibodies		
Mouse monoclonal anti-NF-κB p65 (clone L8F6)	Cell Signaling Technology	Cat# 6956; RRID: AB_10828935
Chemicals, peptides, and recombinant proteins		
Lipopolysaccharide (LPS)	Sigma	Cat# L4130
Phosphate buffered saline (PBS)	Corning	Cat# 21-030-CV
Quinine hydrochloride	Sigma	Cat# Q1125; CAS# 6119-47-7
Sucrose	Sigma	Cat# S9378; CAS# 57-50-1
Denatonium	Sigma	Cat# D5765; CAS# 3734-33-6
Cycloheximide	Calbiochem	Cat# 239763; CAS# 66-81-9
$MgSO_4$	Sigma	Cat# M7506; CAS# 7487-88-9
Glucose	Sigma	Cat# G7528; CAS# 50-99-7
Sucralose	Sigma	Cat# 69293; CAS# 56038-13-2
Saccharin	Sigma	Cat# S1002; CAS# 82385-42-0
Inosine-5′-monophosphate (IMP)	Sigma	Cat# I4625; CAS# 352195-40-5
Monopotassium glutamate (MPG)	Sigma	Cat# 49601; CAS# 6382-01-0
NaCl	Sigma	Cat#S3014; CAS# 7647-14-5
Amiloride	Sigma	Cat# A7410; CAS# 2016-88-8
HCl	Fisher Scientific	Cat# A144-500; CAS# 7647-01-0
Citric acid	Sigma	Cat# C0759; CAS# 77-92-9
NH_4Cl	Sigma	Cat# A4514; CAS# 12125-02-9
Tween20	Sigma	Cat# 11332465001;
NP40	Sigma	Cat# 11332473001
Trypsin-EDTA (0.25%)	Gibco ™/ThermoFisher Scientific	Cat# 25200-056
Fetal bovine serum	Sigma	Cat# F2442
Bovine serum albumin (BSA)	Sigma	Cat# A3059
Digitonin	Promega	Cat# G9441
Trypan blue solution (0.4%)	Corning	Cat# 25-900-CI
Nuclei buffer	10X Genomics	Cat# PN2000153
Chromium Single Cell 3′ Reagent kit v3	10X Genomics	Cat# PN-1000075
DMEM/F12 medium	Life Technologies	Cat# 11320033
Matrigel matrix growth factor reduced phenolred free	Corning	Cat# 356231
Epidermal growth factor	Peprotech	Cat# 315-09
Y-27632	Sigma	Cat# Y0503
N2 supplement	ThermoFisher Scientific	Cat# 17502048
B27 supplement	ThermoFisher Scientific	Cat# 17504044
Critical commercial assays		
Absolutely RNA Microprep Kit	Agilent	Cat# 400805
Superscript III reverse transcriptase kit	Thermo Fisher Scientific	Cat# 18080044
Power SYBR Green PCR Master Mix	Thermo Fisher Scientific	Cat# 4367659
SimpleChIP Kit (Magnetic Beads)	Cell Signaling Technology	Cat# 9003

(*Continued on next page*)

Continued

REAGENT or RESOURCE	SOURCE	IDENTIFIER
Deposited data		
scATAC-seq sequencing data	This paper	GEO: GSE213404
Experimental models: Organisms/strains		
C57BL/6J male and female mice	The Jackson Laboratory	Strain # 000664
Oligonucleotides		
Primers for *β-Actin*, see Table S2	Feng et al., 2012[66]	N/A
Primers for *Nfkb1*, see Table S2	Feng et al., 2020[61]	N/A
Primers for *Tas2rs*, see Table S2	Xu et al., 2013[74]	N/A
Primers for *Trpm5*, see Table S2	This paper	NA
Primers for the *Tnf* Promoter, see Table S2	This paper	N/A
Primers for the promoters of *Tas2r102* and *Tas2r116*, see Table S2	This paper	N/A
Software and algorithms		
PowerLab system	AD Instruments	Colorado Springs, CO, USA
StepOnePlus	Thermo Fisher Scientific	https://www.thermofisher.com
R version 4.1.3	John Chambers	https://www.r-project.org/
Ubuntu 20.04.4 LTS	The Ubuntu Community	https://ubuntu.com/
Loupe Browser	10x Genomics	https://www.10xgenomics.com/products/loupe-browser
Cell Ranger ATAC pipeline v.1.2.0	10x Genomics	https://support.10xgenomics.com/single-cell-atac/software/pipelines/latest/installation
ArchR v1.0.2 package	Granja et al., 2021[23]	https://www.archrproject.com
MACS2 v2.2.7.1	Gaspar, 2018[75]	https://github.com/macs3-project/MACS/wiki/Install-macs2
g:Profiler	Raudvere et al., 2019[44]	https://biit.cs.ut.ee/gprofiler/gost
Cytoscape version 3.9.1	The Cytoscape Consortium	https://cytoscape.org
Other		
Gustometers	Dilog Instruments, Tallahassee, FL	Davis MS-160 mouse gustometers
StepOnePlus Real-Time PCR System	ThermoFisher Scientific	https://www.thermofisher.com
Illumina HiSeq 4000	Ilumina	https://www.illumina.com/systems/sequencing-platforms/hiseq-3000-4000.html

RESOURCE AVAILABILITY

Lead contact

Further information and requests for reagents may be directed to and will be fulfilled by the lead contact Hong Wang (hwang@monell.org).

Materials availability

This study did not generate new unique reagents.

Data and code availability

- Original scATAC-seq data have been deposited at GEO (GSE213404) and are publicly available as of the date of publication. Accession number is listed in the key resources table.
- All original code has been deposited at GitHub and is publicly available (https://github.com/Cailu086Lin/scATACseq_mouse_taste).

- Any additional information required to reanalyze the data reported in this paper is available from the lead contact upon request.

EXPERIMENTAL MODEL AND SUBJECT DETAILS

Animals

All procedures involving mice were performed according to protocols approved by the Monell Chemical Senses Center Institutional Animal Care and Use Committee. Adult male and female C57BL/6J mice were purchased from the Jackson Laboratory and housed in a climate-controlled environment at the animal facility of the Monell Chemical Senses Center. For induction of inflammation, LPS (2.5 mg/kg in PBS) or PBS (a vehicle control) was given by intraperitoneal injection.

Taste organoid culture

Single cell suspension was prepared from circumvallate papillae of 2-6-month-old C57BL/6J mice following published procedure.[63,76] For each batch of taste organoids, five mice were used to generate organoids. Cells were cultured in DMEM/F12 medium (Life Technologies no. 11320033) with 8% Matrigel matrix (Corning) and supplemented with epidermal growth factor (PeproTech), N2 (ThermoFisher Scientific), B27 (ThermoFisher Scientific), Y-27632 (Sigma), and conditional medium containing Wnt3a, R-spondin, and Noggin. Organoids were maintained in ultra-low attachment tissue culture dishes (Corning). Mature taste organoids from early passages that had been cultured for more than 12 days were used. Organoids were treated with LPS (1 μg/ml) for 72 h before harvesting for ChIP-qPCR experiments.

METHOD DETAILS

Brief-access behavioral tests

Brief-access tests were performed using Davis MS-160 mouse gustometers (Dilog Instruments, Tallahassee, FL).[77] Adult mice (age and sex matched) were trained for brief-access tests several days before LPS or PBS injection. The following taste compounds were tested: quinine hydrochloride (0.1, 0.3, and 3 mM) and sucrose (0.1, 0.2, and 0.6 M). To motivate sampling of taste solutions, mice were water-deprived for 22.5 h before the 30-min training sessions and the 30-min test sessions for the bitter taste compound quinine and were food- and water-restricted (1 g of food and 1.5 mL of water) for 23.5 h before test sessions for the sweet taste compound sucrose. In each test session, mice were tested with three different concentrations of the taste compound along with a water control. Water and taste compound solutions were randomly presented to mice following random presentation schemes generated by the computer software. LPS-treated mice and control mice were tested at the same time in parallel: on day 2 and day 4 after LPS or PBS injection, mice were tested with sucrose solutions, and on day 3, with quinine solutions. For data analyses, lick ratios were calculated by dividing the number of licks for taste compounds by the number of licks for water presented in the same test session. For tests of quinine, aversion scores were calculated as 1 – lick ratio. We used repeated ANOVA to compare the between-group effect (PBS vs. LPS), with the taste stimulus concentrations treated as within-group effects, followed by post hoc t-test.

Gustatory nerve recordings

Chorda tympani and glossopharyngeal nerve recordings were carried out as described below.[77] Mice were anesthetized with pentobarbital (50–60 mg/kg of body weight, i.p.), and the trachea was cannulated. Mice were then fixed in the supine position with head holders. For recordings from the chorda tympani nerve, the right nerve was exposed at its exit from the lingual nerve and cut near its entrance to the bulla. For recordings from the glossopharyngeal nerve, the right nerve was exposed by removal of the digastric muscle and posterior horn of the hyoid bone and then dissected free from underlying tissues and cut near its entrance to the posterior lacerated foramen. For whole-nerve recording, the entire nerve was placed on a platinum wire recording electrode. An indifferent electrode was positioned nearby in the wound. Neural responses resulting from chemical stimulations of the tongue were fed into an amplifier (Grass Instruments, West Warwick, RI), monitored on an oscilloscope and an audio monitor. Whole-nerve responses were integrated with a time constant of 1.0 s and recorded using a computer for later analysis using a PowerLab system (PowerLab/sp4; AD Instruments, Colorado Springs, CO).

The following solutions were used as stimuli: 0.1–20 mM quinine hydrochloride, 0.1–30 mM denatonium, 0.003–0.5 mM cycloheximide, 3–300 mM $MgSO_2$, 10–1000 mM sucrose, 30–1000 mM glucose, 0.3–30 mM sucralose, 0.3–20 mM saccharin, 0.1–10 mM inosine-5′-monophosphate (IMP), 10–1000 mM

monopotassium glutamate (MPG) with or without 0.5 mM IMP, 10-1000 mM NaCl with or without 0.1 mM amiloride, 0.1–10 mM HCl, 1–100 mM citric acid, and 100 mM NH_4Cl. These chemicals were dissolved in distilled water and used at ~24°C. During recordings the test solutions were flowed for 30 s (chorda tympani recordings) or 60 s (glossopharyngeal recordings) at the same flow rate and temperature as distilled water used for rinsing the tongue (~0.1 mL/s). The tongue was rinsed with distilled water for 1 min between successive stimulations.

To analyze whole-nerve responses to each stimulus, the magnitudes of integrated responses at different time points after stimulus onset were measured and averaged. The relative response magnitude for each test stimulus was calculated against the response magnitude to 100 mM NH_4Cl, and this value was used for statistical analysis (ANOVA with post hoc t test) and for plotting dose-response curves. For chorda tympani recordings, 6–12 mice per group were used; for glossopharyngeal recordings, 5–10 mice per group were used.

qRT-PCR

At various time points after PBS and LPS injection, mice were euthanized and tongue epithelium was peeled off.[16] Circumvallate and foliate epithelia containing taste buds were cut and pooled together. Total RNA was extracted using Absolutely RNA Microprep Kit (Agilent) and then reverse transcribed into cDNA using Superscript III reverse transcriptase (Thermo Fisher Scientific). qPCR reactions were set up using Power SYBR Green PCR Master Mix (Thermo Fisher Scientific) in duplicate or triplicate and run on a StepOnePlus Real-Time PCR System (Thermo Fisher Scientific). Relative quantification of gene expression was performed using StepOnePlus software based on the $2^{-\Delta\Delta Ct}$ method. β-Actin was used as the endogenous control gene for these analyses. The specificity of the PCR reactions was analyzed by dissociation studies and confirmed by agarose gel electrophoresis. RT-PCR primers are listed in Table S2. Most primers for *Tas2rs* were published previously[74] and several primers were designed for this study (See key resources table and Table S2). For statistical analysis, t-test was conducted, with $p < 0.05$ considered significant.

Isolation of nuclei, preparation of scATAC-seq libraries, and high-throughput sequencing

To isolate the nuclei for scATAC-seq, the peeled tongue epithelia from PBS- and LPS-treated mice were prepared.[16] Six mice per group were used. Epithelia from circumvallate papillae were cut off and rinsed in calcium-free Tyrode's buffer (140 mM NaCl, 5 mM KCl, 10 mM HEPES, 1 mM $MgCl_2$, 10 mM glucose, 10 mM Na-pyruvate, 2 mM EGTA, pH 7.4). Circumvallate epithelia were then transferred to a solution containing 0.25% trypsin-EDTA (Fisher Scientific) and incubated at 37°C for 15 min. Cold Opti-MEM with 10% fetal bovine serum (FBS) (Thermo Fisher Scientific) was added to the mixture, and cells were further dissociated by gentle pipetting. Cells were centrifuged, rinsed with cold Opti-MEM with 10% FBS, passed through a 40 μm cell strainer, and rinsed once with wash buffer (10 mM Tris-HCl, pH 7.5, 10 mM NaCl, 3 mM $MgCl_2$, 1% bovine serum albumin (BSA), and 0.1% Tween20). Dissociated cells were then resuspended in 0.1x Lysis buffer (10 mM Tris-HCl, pH 7.5, 10 mM NaCl, 3 mM $MgCl_2$, 0.9% BSA, 0.01% Tween20, 0.01% NP40, 0.001% digitonin) and incubated on ice for 5 min. Cell lysis was monitored by staining with trypan blue solution (0.4%; Thermo Fisher Scientific). Nuclei were rinsed with wash buffer, centrifuged, resuspended in 1x nuclei buffer (10x Genomics), and counted. About 4000 nuclei per group were used for downstream ATAC-seq procedures.

The chromatin transposition reaction, nuclei partitioning, barcoding, and library construction were carried out at the Next-Generation Sequencing Core (NGSC) facility at the University of Pennsylvania using 10x Genomics Chromium scATAC reagent kits and instruments, following the manufacturer's protocols. High-throughput sequencing was also performed at the NGSC using Illumina HiSeq 4000 instruments.

Data processing with Cell Ranger ATAC pipeline

Demultiplexed raw base call files generated from sequencing were used as inputs to the 10x Genomics Cell Ranger ATAC pipeline (version 1.2.0). FASTQ files were generated and aligned to the mm10 (i.e., GRCm38) mouse genome assembly using the Burrows-Wheeler Aligner Maximal Exact Matches (BWA-MEM) algorithm.[78] Total numbers of reads were 236,312,328 bp and 246,253,784 bp for PBS- and LPS-treated mice, respectively. Fragment files were generated containing all unique properly paired and aligned fragments with mapping quality (MAPQ) > 30. The start and the end of the fragments were adjusted (4 bp from the leftmost alignment position and backward 5 bp from the rightmost alignment position) to account for the 9-bp overhang region that the transposase enzyme occupies during transposition. The adjusted

positions represent the center point between these cuts, and this position is recorded as a cut site that represents a chromatin accessibility event.

Before further data analyses, we previewed the Cell Ranger ATAC pipeline processed data with the Loupe Browser (10x Genomics), an interactive visualization software.

Data analyses with the ArchR pipeline

The downstream data analysis was conducted with ArchR[23] version 1.0.2 pipeline in R (version 4.1.3) using Ubuntu 20.04.4 LTS. Fragment files generated from the Cell Ranger ATAC pipeline were loaded into the ArchR pipeline to create arrow files. We filtered the scATAC-seq data to keep those that had at least 1000 unique nuclear fragments and a TSS enrichment score of 4. During creation of the arrow files, we generated the metadata and matrices, which included a "TileMatrix" (containing insertion counts across genome-wide 500-bp bins) and a "GeneScoreMatrix" that stores the predicted gene expression scores based on weighting of insertion counts in tiles close to a gene promoter (see below). Potential doublets (i.e., a single droplet containing more than one cell) were identified and filtered out, which accounted for 3.5% and 4.2% of the cells from the PBS and LPS samples, respectively.

To minimize batch effects, the ATAC-seq batches for the PBS and LPS samples were merged and calculated for the latent semantic index (LSI), which uses a term frequency (TF) that has been depth normalized to a constant (10,000) followed by further normalization with the inverse document frequency (IDF), and then the resultant matrix was log-transformed (i.e., log(TF – IDF)). Using the iterative LSI approach,[79] we computed an initial LSI transformation on the most accessible tiles. We next applied *Harmony*[80] to regress out the batch effect, resulting in a new harmonized co-embedding.

For clustering and visualization, we used a graph clustering approach (*addCluster* function) by including the dimensionality reduction matrix "Harmony" to identify clusters of the merged samples (PBS+LPS) and then visualized the scATAC-seq data using UMAP dimensionality reduction technique.

For gene score calculation, we used the *addGeneScoreMatrix* function and calculated a gene score matrix for each arrow file at the time of creation. Each sample was independently computed for the counts of each tile (genome-wide fragment bins) per cell. 500 bp of the tile size was used for binning counts prior to gene activity score calculation and the maximum counts per tile allowed is 4. The gene model used for weighting peaks for gene score calculation was "exp(-abs(x)/5000) + exp(-1)", where x is the stranded distance from the transcription start site of the gene, and exp and abs stand for exponential and absolute value, respectively. For sparse scATAC-seq data, the MAGIC imputation method[81] was used to impute gene scores by smoothing signal across nearby cells.

For cell cluster annotation, we used the gene scores from the merged data for the PBS and LPS samples as input matrix. Across all features, each cell cluster was compared to its own background group of cells (all other clusters) to determine if the given cell cluster retains significantly higher accessibility. This procedure was done using *getMarkerFeatures* function. A cutoff threshold of false discovery rate (FDR)-corrected $p < 0.01$ and $\log_2$-transformed fold change (log2FC) > 1.25 was applied to identify genes that appear to be uniquely active in each celltype (Table S3). This gene list was used to manually annotate the cell types.

To calculate the Simpson diversity index, we employed Simpson's index of diversity (*D*), which presents as (1 – *D*) and ranges between 0 and 1, with greater values indicating larger sample diversity. We used Simpson's index to characterize the composition of all cells across the identified 11 cell types for the PBS and LPS samples separately.

For peak calling, we created pseudo-bulk replicates to group single cells such that the data from each single cell were combined into a single pseudo-sample that resembled a bulk ATAC-seq experiment. We performed peak calling for each cluster independently to get high-quality, fixed-width, nonoverlapping peaks that represent the epigenetic diversity of PBS and LPS samples. Briefly, fragments from cells were grouped by broad cell class, and peaks were called on all cluster fragments using MACS2.[75] Peaks from each celltype were then combined, merging overlapping peaks (overlapping peaks called within a single sample were handled using an iterative removal procedure) to form a union peak set, and a cell-by-peak matrix was binarized for all downstream applications.

For co-accessibility analysis, we calculated correlations in accessibility between two peaks across many single cells to identify cell-type-specific peaks as being co-accessible, because these peaks are often all accessible together within a single celltype and often all not accessible in all other cell types. We applied the function *addCoAccessibility* to cells from the merged PBS and LPS dataset and then to the PBS and LPS datasets separately, and reported data from the PBS dataset only.

Differentially accessible peaks for each celltype between the PBS and LPS samples were determined by performing a two-sided Wilcoxon signed-rank test and selecting peaks that had log-transformed fold change >0.5 and FDR-corrected $p < 0.05$.

For transcription factor motif enrichment analysis and footprinting, we used Catalog of Inferred Sequence Binding Preferences (CIS-BP) motifs obtained from chromVAR motifs mouse_pwms_v2[82] to calculate motif positions using *motifmatchr* in ArchR. We first added the motif matrix in the object of the control PBS sample, next used differential testing to define the set of significantly differential peaks of all cell types for motif enrichment, and then performed hypergeometric enrichment of a given peak annotation within the defined marker peaks. We sorted out the motif for peaks with log-transformed fold change >0.3 and FDR-corrected $p < 0.5$ as cell-type-specific motif enrichment. Footprinting plots of the cell-type-specific motifs were generated using a normalization method that subtracts the Tn5 bias from the footprinting signal, because the insertion sequence bias of the Tn5 transposase could lead to misclassification of transcription factor footprints.

To identify potential positive transcriptional regulators, we first identified deviant transcription factor motifs by performing a ChromVAR deviation analysis. The deviation score (Zscore) was predicted for enrichment of transcription factor activity on a per-cell basis from sparse chromatin accessibility data with the GC-content bias correction. Using the motif and gene score matrix, we identified transcription factors whose motif accessibilities were correlated with their own gene score. We filtered the positive regulators as those whose correlation between the motif enrichment and the gene score was >0.5 with an FDR-adjusted pvalue <0.01 and a maximum inter-cluster difference in deviation Zscore in the top quartile. This analysis was done with the PBS dataset only.

To identify differentially regulated transcription factors by LPS, we statistically compared the PBS (control) and LPS samples to identify the up- and down-regulators and motifs in differentially accessible peaks in the C1 (type I taste cells), C3 (taste stem/progenitor 1), and C7 (taste stem/progenitor 2) clusters. The cutoff thresholds log-transformed fold change >0.5 and FDR-corrected $p < 0.1$ were applied in the two-sided Wilcoxon signed-rank tests.

Pathway enrichment analysis

Pathway enrichment analyses were done as described by Reimand et al. (2019).[83] Marker genes from each cell cluster (FDR <0.01 and log2FC > 0.5) were analyzed separately. For analysis of LPS-induced changes in gene scores, up- and down-regulated genes (FDR <0.05 and log2FC > 0.5 or <−0.5) were analyzed separately. Gene lists were first analyzed in g:Profiler, excluding electronic Gene Ontology (GO) annotations and limiting gene terms to 5–1000. Enriched pathways identified by g:Profiler from GO molecular functions and GO biological processes were imported into Cytoscape software (version 3.9.1) and visualized using EnrichmentMap. Functionally connected pathways were further manually organized into groups for better visualization and interpretation.

ChIP-qPCR experiment

ChIP was performed using the SimpleChIP kit (Magnetic Beads, Cell Signaling Technology) following the manufacturer's protocol. Seeded taste organoids were treated with LPS (1 μg/ml) for 72 h. Crosslinking was done in the culture dishes with 1% formaldehyde for 10 min at room temperature. Glycine was then added into the mixture (final 1X) and incubated for 5 min at room temperature. Cells were then washed with cold PBS and then collected by scraping and centrifuged. Nuclei preparation and chromatin digestion were then done following the protocol from the kit. The size of the digested DNA was monitored by gel electrophoresis. Chromatin immunoprecipitation was done with a monoclonal antibody against NF-κB p65 (Cell Signaling). Normal rabbit IgG and an antibody against histone H3, both provided by the kit, were used as the negative and positive controls, respectively. Eluted chromatin was purified using spin columns provided by the kit. qPCR was performed using Power SYBR Green PCR Master Mix (ThermoFisher Scientific)

with primers to the promoter regions of *Tnf*, *Tas2r102*, and *Tas2r116* (Table S2). Fold enrichment was calculated by comparing to the negative control samples.

QUANTIFICATION AND STATISTICAL ANALYSIS

Results for behavioral tests, nerve recordings, and PCRs are shown as means ± SEM. $p < 0.05$ was considered as significantly different. Statistical analysis was performed using ANOVA or Student's *t* test (two-tailed) in either R version 4.1.3 or Prism 9.5. Details for statistical analysis of scATAC-seq data can be found under Data analyses with the ArchR pipeline in the method details section. Additional details are provided in the figure legends.